Multiscale Model. Simul.
Vol. 9, No. 2, pp. 872–903

PARTITIONED ANALYSIS FOR DIMENSIONALLY-HETEROGENEOUS HYDRAULIC NETWORKS*

JORGE S. LEIVA†, PABLO J. BLANCO‡, AND GUSTAVO C. BUSCAGLIA§

Abstract. In this work an iterative strategy is developed to tackle the problem of coupling dimensionally-heterogeneous models in the context of fluid mechanics. The procedure proposed here makes use of a reinterpretation of the original problem as a nonlinear interface problem for which classical nonlinear solvers can be applied. Strong coupling of the partitions is achieved while dealing with different codes for each partition, each code in black-box mode. The main application for which this procedure is envisaged arises when modeling hydraulic networks in which complex and simple subsystems are treated using detailed and simplified models, correspondingly. The potentialities and the performance of the strategy are assessed through several examples involving transient flows and complex network configurations.

Key words. strong coupling, dimensionally-heterogeneous models, incompressible flows, partitioned analysis, domain decomposition

AMS subject classifications. 76D05, 76M10, 65M22, 65M55

DOI. 10.1137/100809301

1. Introduction.

The coupling of models of different dimensionality in fluid dynamics was first addressed in [17]. Alternative formulations and applications have been presented subsequently in the context of computational hemodynamics [2], [4], [5], [8], [10], [14], [19], [22], proving the usefulness of such an approach to model complex systems. Generally speaking, such a situation arises when a complex system, such as a hydraulic network, is split into different subsystems with different characteristic geometrical scales. Complex components of the system must be modeled using the full Navier–Stokes equations, whereas some approximation is acceptable in other, simpler components, such as long pipes or valves, for example. In general, the global dynamics results from the interaction among the parts of the whole network, requiring the use of coupled
dimensionally-heterogeneous models.

The first approaches to deal in an iterative manner with the coupling of dimensionally-heterogeneous models were based on an explicit approach [16] as well as on basic Dirichlet-to-Neumann (Gauss–Seidel) iterations with relaxation [2], [8], [18]. Nevertheless, it is well known that tuning the iterates by setting proper relaxation parameters does not follow a general procedure, and situations for which the algorithm fails may easily be encountered. Recently, a more robust methodology based on the Schur complement has been proposed for the related problem of imposing flow rate boundary conditions [20] (see also [21]).

*Received by the editors September 21, 2010; accepted for publication (in revised form) April 15, 2011; published electronically June 30, 2011. This work was partially supported by the National Institute of Science and Technology in Medicine Assisted by Scientific Computing (INCT–MACC), Brazil. This work was also partially supported by the Brazilian agencies CNPq, FAPERJ, and FAPESP.

http://www.siam.org/journals/mms/9-2/80930.html

†Instituto Balseiro, Av. Bustillo Km. 9.5, San Carlos de Bariloche, 8400, Río Negro, Argentina (leivaj@ib.cnea.gov.ar).

‡Laboratório Nacional de Computação Científica, Av. Getúlio Vargas 333, Quitandinha, 25651-075, Petrópolis, RJ, Brazil (pjblanco@lncc.br).

§Instituto de Ciências Matemáticas e de Computação, Universidade de São Paulo, Av. do Trabalhador Sãocarlense 400, 13560-970 São Carlos, SP, Brazil (gustavo.buscaglia@icmc.usp.br).

The motivation for establishing robust iterative strong coupling techniques lies in the need for employing well validated codes, suitably devised for systems with very different dynamics, such as black boxes. The technique presented here can be understood as a domain decomposition approach where the partitioning takes place at the coupling interfaces among models of different dimensionality. The idea of the iterative strategy presented here stems from the developments presented by Leiva, Blanco, and Buscaglia in [15] for heat conduction problems, and further extended in [3] to one-dimensional (1D) networks made of deformable pipes such as the arterial tree. In this work we go back to dimensionally-heterogeneous situations and extend the previous algorithm as needed by the Navier–Stokes equations, viewed as a nonlinear evolution problem. Basically, the original monolithic problem is understood as an interface problem in terms of interface variables. The reinterpretation of the Dirichlet-to-Neumann algorithm applied for this problem as a Gauss–Seidel method plays a crucial role, since it allows us to change the resolution process to more robust and sophisticated iterative methods. In [15] the GMRES iterative procedure was the approach chosen to solve the problem. Here, the extension to nonlinear problems is carried out by employing either the Broyden method or the Newton-GMRES algorithm. Different situations are assessed, and the performance of specific variants of these algorithms is discussed.

This work is organized as follows. Section 2 presents the original problem. The coupling strategy is explained in detail in section 3, while several numerical results are presented in section 4. Finally, the main conclusions are drawn in section 5.

2. Coupled dimensionally-heterogeneous models. This section presents the basic elements in the formulation of the problem of coupling dimensionally-heterogeneous models. Also, the reduction of this problem to a problem involving the imposition of flow rate boundary conditions is performed. For a thorough derivation of the models that will be presented here the reader is referred to [2], [8], [9], [12].

For the flow models presented in this section we assume incompressibility of the fluid and also rigidity of the pipes. This is by no means restrictive from the point of view of the domain decomposition approach. Indeed, compliant vessels are explored in the last example, showing the applicability of the methodology to hemodynamics problems. This is why the formulation is not oversimplified in some parts where it could be, but it is presented in a more general framework so as to embrace more general situations like the one encountered in hemodynamics.

2.1. Mathematical model. In order to introduce the model we resort to the simplest situation shown in Figure 2.1 where the interaction between two systems with different leading geometrical scales is shown. Also, we employ graph notation, denoting by $\mathcal{N}$ the nodes (or complex models), by $\mathcal{C}$ the connections (or simple models), and by $\mathcal{I}$ the coupling interfaces. The *Times* font is used for the elements described with the calligraphic font within the text.

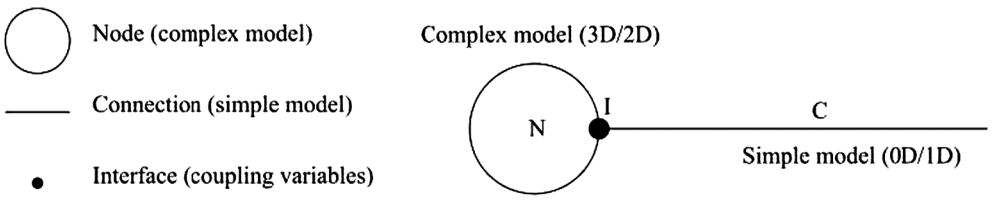

FIG. 2.1. *Coupled system consisting of two geometrical scales.*

System $\mathcal{N}$ has complex dynamics and is modeled via the full Navier–Stokes equations (two-dimensional (2D) or three-dimensional (3D)), and thus $\mathcal{N}$ denotes a spatial domain $\mathbf{\Omega} \in \mathbb{R}^n$ $(n = 2, 3)$. In order to have existence and uniqueness of the solution we will always assume that the data is sufficiently small. In turn, system $\mathcal{C}$ has simple dynamics and is represented through the condensed Navier–Stokes equations (in particular, it can be zero-dimensional (0D) models when no change of area is considered or 1D models when the pipes are deformable).

Over the coupling interface $\mathcal{I}$, which denotes a given portion of the boundary $\partial\mathbf{\Omega}$ of $\mathbf{\Omega}$, continuity of mean velocity (or, equivalently, mass flow) and of normal traction assumed to hold. The governing equations are (here we consider 0D models for the simple components)

$$
\begin{cases}
\rho \frac{\partial \mathbf{u}}{\partial t} + \rho(\nabla \mathbf{u})\mathbf{u} + \nabla p - \mu \Delta \mathbf{u} = 0 & \text{in } \mathcal{N}, \\
\operatorname{div} \mathbf{u} = 0 & \text{in } \mathcal{N}, \\
\mathbf{u} = 0 & \text{on } \partial\mathbf{\Omega} \setminus \Gamma, \\
Q_1 = -\int_\Gamma \mathbf{u} \cdot \mathbf{n} \mathrm{d}\Gamma & \text{in } \mathcal{I}, \\
-P_1 \mathbf{n} = \frac{1}{|\Gamma|} \int_\Gamma (-p\mathbf{I} + \mu(\nabla \mathbf{u} + (\nabla \mathbf{u})^T))\mathbf{n} \mathrm{d}\Gamma & \text{in } \mathcal{I}, \\
M \frac{dQ_1}{dt} + K Q_1 - (P_2 - P_1) - B = 0 & \text{in } \mathcal{C}, \\
Q_1 + Q_2 = 0 & \text{in } \mathcal{C}, \\
P_2 = P_{\text{ref}} & \text{in } \mathcal{O},
\end{cases}
\tag{2.1}
$$

where Γ is the coupling interface corresponding to $\mathcal{I}$ with unit outward normal $\mathbf{n}$ (seen from system $\mathcal{N}$), $(\mathbf{u}, p)$ is the pair velocity-pressure in $\mathcal{N}$, and ρ and μ are the density and dynamic viscosity. Note that a Dirichlet boundary condition is imposed over the complementary boundary to the coupling interface $\partial\mathbf{\Omega} \setminus \Gamma$. Also, Q_1 and Q_2 are the flow rates at both boundaries (ends) of the $\mathcal{C}$ component. Note here that just one flow rate should be necessary; however, as said before, we keep both quantities so the ideas can be straightforwardly applied to more general contexts. The drop pressure is given by $\Delta P = P_2 - P_1$, noting that here we impose a pressure boundary condition to this component given by P_{ref} at the outlet boundary of the network, denoted by $\mathcal{O}$. Finally, B is a source term that represents a pump acting in such connection, and M and K are the inertial and friction coefficients, which read as

$$
\begin{aligned}
M &= \frac{\rho L}{A}, \\
K &= \frac{8\pi\mu L}{A^2} \qquad \text{circular pipe}, \\
K &= \frac{12\mu L}{a^3 H} \qquad \text{parallel plates},
\end{aligned}
\tag{2.2}
$$

where L is the length of the pipe, A is the sectional area of the pipe (in the case of a circular pipe), and a is the separation between plates with depth equal to H (in the case of parallel plates). Over Γ continuity of flow rate and continuity of mean traction are considered.

The problem stated by (2.1) is, however, not well posed. We thus make the choice

$$
\frac{1}{|\Gamma|} \int_\Gamma (-p\mathbf{I} + \mu(\nabla \mathbf{u} + (\nabla \mathbf{u})^T))\mathbf{n} \mathrm{d}\Gamma = (-p\mathbf{I} + \mu(\nabla \mathbf{u} + (\nabla \mathbf{u})^T))\mathbf{n} \qquad \text{in } \mathcal{I},
\tag{2.3}
$$

which implies that the quantity $(-p\mathbf{I} + \mu(\nabla \mathbf{u} + (\nabla \mathbf{u})^T))\mathbf{n}$ is constant across Γ. With this choice we are making use of the do-nothing approach, and therefore we recover uniqueness (see [12]) so that we end up with the following problem for the coupled,

dimensionally-heterogeneous system:

$$
\begin{cases}
\rho \frac{\partial \mathbf{u}}{\partial t} + \rho(\nabla \mathbf{u})\mathbf{u} + \nabla p - \mu \Delta \mathbf{u} = 0 & \text{in } \mathcal{N}, \\
\operatorname{div} \mathbf{u} = 0 & \text{in } \mathcal{N}, \\
\mathbf{u} = 0 & \text{on } \partial\Omega \setminus \Gamma, \\
Q_1 = -\int_\Gamma \mathbf{u} \cdot \mathbf{n} \mathrm{d}\Gamma & \text{in } \mathcal{I}, \\
-P_1 \mathbf{n} = (-p\mathbf{I} + \mu(\nabla \mathbf{u} + (\nabla \mathbf{u})^T))\mathbf{n} & \text{in } \mathcal{I}, \\
M \frac{dQ_1}{dt} + K Q_1 - (P_2 - P_1) - B = 0 & \text{in } \mathcal{C}, \\
Q_1 + Q_2 = 0 & \text{in } \mathcal{C}, \\
P_2 = P_{\text{ref}} & \text{in } \mathcal{O}.
\end{cases} \tag{2.4}
$$

In order to treat the different components following a black-box approach we choose now the interface variables as being (Q^1, P^1), that is, the flow rate and pressure at the coupling interface. With this, the problem is augmented and reads as

$$
\begin{cases}
\rho \frac{\partial \mathbf{u}}{\partial t} + \rho(\nabla \mathbf{u})\mathbf{u} + \nabla p - \mu \Delta \mathbf{u} = 0 & \text{in } \mathcal{N}, \\
\operatorname{div} \mathbf{u} = 0 & \text{in } \mathcal{N}, \\
\mathrm{u} = 0 & \text{on } \partial\Omega \setminus \Gamma, \\
Q_{\mathcal{N},1} = -\int_\Gamma \mathbf{u} \cdot \mathbf{n} \mathrm{d}\Gamma & \text{in } \mathcal{I}, \\
-P_{\mathcal{N},1} \mathbf{n} = (-p\mathbf{I} + \mu(\nabla \mathbf{u} + (\nabla \mathbf{u})^T))\mathbf{n} & \text{in } \mathcal{I}, \\
Q^1 + Q_{\mathcal{N},1} = 0 & \text{in } \mathcal{I}, \\
P^1 - P_{\mathcal{N},1} = 0 & \text{in } \mathcal{I}, \\
Q^1 - Q_{\mathcal{C},1} = 0 & \text{in } \mathcal{I}, \\
P^1 - P_{\mathcal{C},1} = 0 & \text{in } \mathcal{I}, \\
M \frac{dQ_{\mathcal{C},1}}{dt} + K Q_{\mathcal{C},1} - (P_{\mathcal{C},2} - P_{\mathcal{C},1}) - B = 0 & \text{in } \mathcal{C}, \\
Q_{\mathcal{C},1} + Q_{\mathcal{C},2} = 0 & \text{in } \mathcal{C}, \\
P_{\mathcal{C},2} = P_{\text{ref}} & \text{in } \mathcal{O},
\end{cases} \tag{2.5}
$$

where we used $(Q_{\mathcal{N},1}, P_{\mathcal{N},1})$ and $(Q_{\mathcal{C},1}, P_{\mathcal{C},1})$ to denote the variables from the complex and simple models that must match the interface state variables (Q^1, P^1).

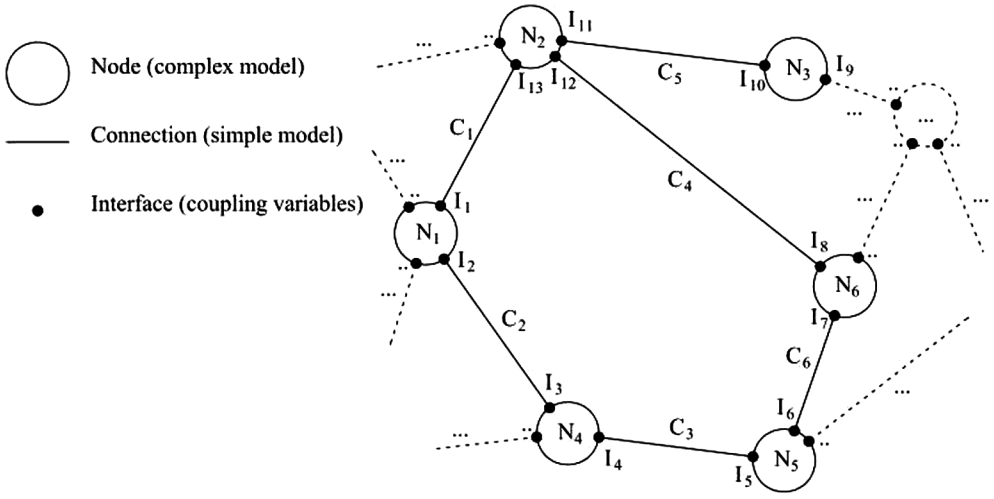

FIG. 2.2. *Scheme of a generic coupled dimensionally-heterogeneous system.*

This system can be extended to a generic graph-like network as shown in Figure 2.2. Let us say that it consists of n_T *nodes* (complex models), c_T *connections* (simple models), i_T *interfaces* (coupling interfaces), and o_T *network outlets*.

Therefore, as happened with (2.5), in this case we have

$$\begin{cases} \rho \frac{\partial \mathbf{u}_n}{\partial t} + \rho(\nabla \mathbf{u}_n)\mathbf{u}_n + \nabla p_n - \mu \Delta \mathbf{u}_n = 0 & \text{in } \mathcal{N}_n, n = 1, \ldots, n_T, \\ \operatorname{div} \mathbf{u}_n = 0 & \text{in } \mathcal{N}_n, n = 1, \ldots, n_T, \\ \mathbf{u}_n = 0 & \text{on } \partial\Omega_n \setminus \Gamma_n, n = 1, \ldots, n_T, \\ Q_{\mathcal{N}_n,l} = -\int_{\Gamma_l} \mathbf{u}_n \cdot \mathbf{n}_l \mathrm{d}\Gamma & \text{on } \Gamma_l, l = 1, \ldots, N_n, n = 1, \ldots, n_T, \\ -P_{\mathcal{N}_n,l}\mathbf{n}_l = (-p_n \mathbf{I} + \mu(\nabla \mathbf{u}_n + (\nabla \mathbf{u}_n)^T))\mathbf{n}_l & \text{on } \Gamma_l, l = 1, \ldots, N_n, n = 1, \ldots, n_T, \\ Q^i + Q_{\mathcal{N}_n,l|\mathcal{I}_i} = 0 & \text{in } \mathcal{I}_i, i = 1, \ldots, i_T, \\ P^i - P_{\mathcal{N}_n,l|\mathcal{I}_i} = 0 & \text{in } \mathcal{I}_i, i = 1, \ldots, i_T, \\ Q^i - Q_{\mathcal{C}_c,k|\mathcal{I}_i} = 0 & \text{in } \mathcal{I}_i, i = 1, \ldots, i_T, \\ P^i - P_{\mathcal{C}_c,k|\mathcal{I}_i} = 0 & \text{in } \mathcal{I}_i, i = 1, \ldots, i_T, \\ M_c \frac{dQ_{\mathcal{C}_c,1}}{dt} + K_c Q_{\mathcal{C}_c,1} - (P_{\mathcal{C}_c,2} - P_{\mathcal{C}_c,1}) - B_c = 0 & \text{in } \mathcal{C}_c, c = 1, \ldots, c_T, \\ Q_{\mathcal{C}_c,1} + Q_{\mathcal{C}_c,2} = 0 & \text{in } \mathcal{C}_c, c = 1, \ldots, c_T, \\ P_{\mathcal{C}_c,k|\mathcal{O}_o} = P^o_{\text{ref}} & \text{in } \mathcal{O}_o, o = 1, \ldots, o_T. \end{cases} \tag{2.6}$$

Here $Q_{\mathcal{C}_c,k|\mathcal{I}_i}$ and $P_{\mathcal{C}_c,k|\mathcal{I}_i}$ are the flow rate and pressure in the simplified model $\mathcal{C}_c$ over the coupling interface $\mathcal{I}_i$ (with $k = 1$, 2 depending on whether $\mathcal{I}_i$ is an inlet or an outlet for the $\mathcal{C}_c$ component). Analogously, $P_{\mathcal{C}_c,k|\mathcal{O}_o}$ is the pressure in the simplified model over the network outlet $\mathcal{O}_o$ (with $k = 1, 2$ depending on whether $\mathcal{O}_o$ is an inlet or an outlet for the $\mathcal{C}_c$ component), which equals the data P^o_{ref}. Likewise, $Q_{\mathcal{N}_n,l|\mathcal{I}_i}$ and $P_{\mathcal{N}_n,l|\mathcal{I}_i}$ are the flow rate and pressure in the complex model $\mathcal{N}_n$ over the local boundary Γ_l, and that corresponds to the coupling interface $\mathcal{I}_i$. We denote by N_n the number of interfaces owned by the complex model $\mathcal{N}_n$, while the number of interfaces owned by the simple model $\mathcal{C}_c$ is trivially $N_c = 2$ (however, more general situations can be considered). Notice that subscripts denote indexes referring to local numeration (component-specific), whereas superscripts refer to indexes in global numeration (interfaces and network outlets).

Remark 1. Problem (2.6) could be simplified by eliminating, for example, the unknowns $Q_{\mathcal{N}_n,l|\mathcal{I}_i}$ and $P_{\mathcal{N}_n,l|\mathcal{I}_i}$. Nonetheless, we keep them in order to put in evidence, when selected, the variables that are going to play the role of boundary conditions in the domain decomposition perspective that will be discussed in section 3.

2.2. On the imposition of flow rate boundary conditions. The problem of imposing flow rate boundary conditions is actually a very particular situation of the problem referred to in the previous section. Consider the scheme shown in Figure 2.3, where a complex model $\mathcal{N}$ consists of one incoming connection and two outgoing connections. Over each connection we know exactly the flow rate, being Q^1, Q^2, and Q^3 such that $\sum_{i=1}^{3} Q^i = 0$.

Indeed, this problem is formulated just by getting rid of the equations that describe the dynamics of the simplified models, because the flow rates Q^i, $i = 1$, 2, 3, are not unknowns here; then

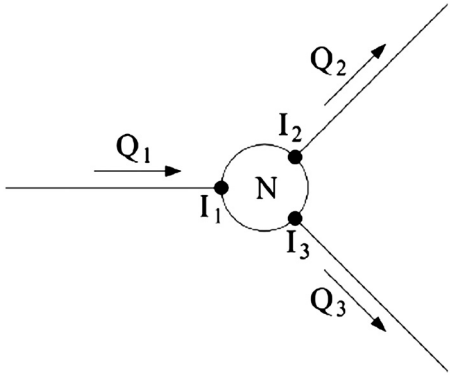

FIG. 2.3. *Complex system with flow rate boundary conditions.*

$$
\begin{cases}
\rho \frac{\partial \mathbf{u}}{\partial t} + \rho(\nabla \mathbf{u})\mathbf{u} + \nabla p - \mu \Delta \mathbf{u} = 0 & \text{in } \mathcal{N}, \\
\operatorname{div} \mathbf{u} = 0 & \text{in } \mathcal{N}, \\
\mathbf{u} = 0 & \text{on } \partial\Omega \setminus \Gamma, \\
Q_{\mathcal{N},l} = -\int_{\Gamma_l} \mathbf{u} \cdot \mathbf{n}_l \mathrm{d}\Gamma & \text{on } \Gamma_l, l = 1,2,3, \\
-P_{\mathcal{N},l}\mathbf{n}_l = (-p\mathbf{I} + \mu(\nabla \mathbf{u} + (\nabla \mathbf{u})^T))\mathbf{n}_l & \text{on } \Gamma_l, l = 1,2,3, \\
Q^i - Q_{\mathcal{N},l|\mathcal{I}_i} = 0 & \text{in } \mathcal{I}_i, i = 1,2,3, \\
P^i - P_{\mathcal{N},l|\mathcal{I}_i} = 0 & \text{in } \mathcal{I}_i, i = 1,2,3.
\end{cases} \tag{2.7}
$$

In this case, Q^i is the known flow rate, while P^i is the resulting normal traction that plays the role of a Lagrange multiplier in order to impose the given flow rate.

Remark 2. The incompresible fluid flow problem in rigid pipes is not well posed if all flow rates are imposed at the inlet/outlet boundaries: (i) if $\sum_{i=1}^{3} Q^i \neq 0$, this is because of the compatibility of the data, whereas (ii) if $\sum_{i=1}^{3} Q^i = 0$, the average pressure is still unknown (actually, can be arbitrarily chosen). In the latter case we need to fix the pressure at some point to have well-posedness. In the case of the whole network (see (2.6)), if the set of outlet boundaries $\mathcal{O}_o$ is empty, then we also need to fix the pressure at some point. The same holds for each local component (3D or 0D) when we split the network in the domain decomposition perspective. Therefore, imposing flow rates at the ends of the connections may give rise to both cases (i) and (ii). For the case of deforming domains (0D, 1D, or 3D) the flow rate can be imposed at all boundaries without any restriction.

3. Partitioned strategy. First, in this section the problem already presented in section 2 is recast in terms of coupling (or interface) variables, presenting the coupling strategy developed in [15] for linear problems and extending it to nonlinear problems like the ones seen in the previous section.

3.1. Interface variables problem. Generally speaking, the choice of the interface variables depends upon the underlying models of a given coupling interface, specifically upon the physical quantities for which some sense of conservation or continuity exists. When dealing with heterogeneous, or nonconforming media, besides the physical considerations other numerical-mathematical conditions have to be taken into account. In particular, the trace of the approximation spaces employed at each side of the coupling interface. It is worth noting that there exist inf-sup-like conditions that pose the necessary requirements, regarding what was said above, to ensure existence and unique-

ness of the solutions of the global system. Nevertheless, we will not delve into these mathematical aspects, which are partially treated in [1], [6].

The simplest choice consists in taking as interface unknowns the variables corresponding to the simplest model among those which share a given coupling interface. In the cases developed in the present work (see section 2) such choice corresponds to flow rate Q^i and pressure P^i, $i = 1, \ldots, i_T$. Hence, when talking about Neumann boundary conditions we understand the imposition of the pressure P^i, while by Dirichlet boundary conditions is understood the imposition of the flow rate Q^i.

Rewriting problem (2.6) in terms of the interface variables $(\{P^i\}_{i=1}^{i_T}, \{Q^i\}_{i=1}^{i_T})$ requires the elimination of the internal degrees of freedom of the system. In order to do so, it is necessary to define the mappings that relate the interface variables among them, in the spirit of the classical Steklov–Poincaré operator found in linear problems. Let us isolate the treatment of each submodel (complex and simple ones). In what follows the numeration of the quantities is given locally, that is, a local numeration for each submodel, without relation with the numeration given in the whole problem (2.6).

First, for each complex model $\mathcal{N}_n$ we have N_n coupling boundaries. It is assumed that there are N_n^Q coupling boundaries where the flow rate is imposed (the data at hand is $(\{Q_{\mathcal{N}_n,j}\}_{j\in S_n^Q})$, S_n^Q being the corresponding set of indexes and N_n^Q its cardinality), whereas N_n^P is the number of coupling boundaries where a Neumann boundary condition, via the value of the pressure, is considered (the data at hand is $(\{P_{\mathcal{N}_n,j}\}_{j\in S_n^P})$, S_n^P being the corresponding set of indexes and N_n^P its cardinality). Then it is $N_n = N_n^Q + N_n^P$. Thus, for each complex model $\mathcal{N}_n$, from problem (2.6), we can write the following abstract functional relation among the unknowns $(\{P_{\mathcal{N}_n,j}\}_{j\in S_n^Q}, \{Q_{\mathcal{N}_n,j}\}_{j\in S_n^P})$ and the data $(\{P_{\mathcal{N}_n,j}\}_{j\in S_n^P}, \{Q_{\mathcal{N}_n,j}\}_{j\in S_n^Q})$ as follows:

$$\begin{bmatrix} \{P_{\mathcal{N}_n,j}\}_{j\in S_n^Q} \\ \{Q_{\mathcal{N}_n,j}\}_{j\in S_n^P} \end{bmatrix} = \mathcal{G}_{\mathcal{N}_n}\left(\begin{bmatrix} \{Q_{\mathcal{N}_n,j}\}_{j\in S_n^Q} \\ \{P_{\mathcal{N}_n,j}\}_{j\in S_n^P} \end{bmatrix} \right). \tag{3.1}$$

Note that there is a time dependence in the definition of the operator $\mathcal{G}_{\mathcal{N}_n}$. This has been disregarded for notational simplicity. The functional relation given by this operator maps, at any time, $\mathbb{R}^{N_n^Q+N_n^P}$ onto itself, that is,

$$\mathcal{G}_{\mathcal{N}_n} : \underbrace{(\mathbb{R}\times\cdots\times\mathbb{R})}_{N_n^Q\text{times}} \times \underbrace{(\mathbb{R}\times\cdots\times\mathbb{R})}_{N_n^P\text{times}} \to \underbrace{(\mathbb{R}\times\cdots\times\mathbb{R})}_{N_n^Q\text{times}} \times \underbrace{(\mathbb{R}\times\cdots\times\mathbb{R})}_{N_n^P\text{times}} \quad \forall\ t, \tag{3.2}$$

and amounts to the solution of the following boundary value problem (for a given complex model $\mathcal{N}_n$):

$$\begin{cases} \rho\frac{\partial \mathbf{u}_n}{\partial t} + \rho(\nabla \mathbf{u}_n)\mathbf{u}_n + \nabla p_n - \mu\Delta\mathbf{u}_n = 0 & \text{in } \mathcal{N}_n, \\ \operatorname{div}\mathbf{u}_n = 0 & \text{in } \mathcal{N}_n, \\ \mathbf{u}_n = 0 & \text{on } \partial\Omega_n \setminus \Gamma_n, \\ -\int_{\Gamma_j} \mathbf{u}_n\cdot\mathbf{n}_j \mathrm{d}\Gamma = Q_{\mathcal{N}_n,j} & \text{on } \Gamma_j, j\in\mathcal{N}_n^Q, \\ -P_{\mathcal{N}_n,j}\mathbf{n}_j = (-p_n\mathbf{I} + \mu(\nabla\mathbf{u}_n + (\nabla\mathbf{u}_n)^T))\mathbf{n}_j & \text{on } \Gamma_j, j\in\mathcal{N}_n^Q, \\ Q_{\mathcal{N}_n,j} = -\int_{\Gamma_j}\mathbf{u}_n\cdot\mathbf{n}_j\mathrm{d}\Gamma & \text{on } \Gamma_j, j\in\mathcal{N}_n^P, \\ (-p_n\mathbf{I} + \mu(\nabla\mathbf{u}_n + (\nabla\mathbf{u}_n)^T))\mathbf{n}_j = -P_{\mathcal{N}_n,j}\mathbf{n}_j & \text{in } \Gamma_j, j\in\mathcal{N}_n^P. \end{cases} \tag{3.3}$$

The mapping $\mathcal{G}_{\mathcal{N}_n}$ relates the imposed boundary conditions with the corresponding unknowns (dual variables). In vector notation expression (3.1) is

$$\begin{bmatrix} \mathbf{P}_{N_n^Q} \\ \mathbf{Q}_{N_n^P} \end{bmatrix} = \mathcal{G}_{\mathcal{N}_n}\left(\begin{bmatrix} \mathbf{Q}_{N_n^Q} \\ \mathbf{P}_{N_n^P} \end{bmatrix} \right), \tag{3.4}$$

where each component of the vector represents a local interface of the complex model $\mathcal{N}_n$.

Remark 3. Suppose that $N_n^P = 0$ ($N_n = N_n^Q$) and that the problem is linear and homogeneous. Then, expression (3.4) becomes

$$\mathbf{P}_{N_n} = \mathcal{G}_{\mathcal{N}_n}^{SP}(\mathbf{Q}_{N_n}), \tag{3.5}$$

which is the classical Steklov–Poincaré operator that, for a given primal quantity, returns the dual variable. Likewise, if $N_n^Q = 0$ ($N_n = N_n^P$), and under the same assumptions, expression (3.4) becomes

$$\mathbf{Q}_{N_n} = [\mathcal{G}_{\mathcal{N}_n}^{SP}]^{-1}(\mathbf{P}_{N_n}). \tag{3.6}$$

Remark 4. Take the case when $N_n^P = 0$, that is, the problem given by expression (3.5) from the previous remark. Such a problem may not be well posed. Indeed, the flow rate information provided as boundary conditions must meet the requirement

$$\sum_{j=1}^{N_n} Q_{\mathcal{N}_n,j} = 0, \tag{3.7}$$

due to the incompressibility constraint, and we have to fix the pressure at some point. Otherwise, the problem does not have a solution. This tells us that the choice of boundary conditions is not always arbitrary. In fact, devising an iterative procedure to solve (3.5) entails evaluating the residual at several iterations. Through the iterations, via an orthonormalization-based algorithm (or Richardson iterations), for instance, the constraint $\sum_{j=1}^{N_n} Q_{\mathcal{N}_n,j} = 0$ is not satisfied in general. Therefore, the iterative procedure is not well posed. This is the same problem as the one commented on in section 2.2 (see Remark 2).

Depending upon the model under study, it is not always possible to find an explicit relation like (3.4), but it is possible to write an implicit relation as follows:

$$\overline{\mathcal{F}}_{\mathcal{N}_n}\left(\begin{bmatrix} \mathbf{P}_{N_n^Q} \\ \mathbf{Q}_{N_n^P} \end{bmatrix}, \begin{bmatrix} \mathbf{Q}_{N_n^Q} \\ \mathbf{P}_{N_n^P} \end{bmatrix} \right) = 0. \tag{3.8}$$

With the purpose of simplifying the notation we reorder the variables as follows:

$$\mathcal{F}_{\mathcal{N}_n}\left(\begin{bmatrix} \mathbf{P}_{N_n^Q} \\ \mathbf{P}_{N_n^P} \end{bmatrix}, \begin{bmatrix} \mathbf{Q}_{N_n^Q} \\ \mathbf{Q}_{N_n^P} \end{bmatrix} \right) = \mathcal{F}_{\mathcal{N}_n}(\mathbf{P}_{N_n}, \mathbf{Q}_{N_n}) = 0. \tag{3.9}$$

Here we have analyzed the complex models. Analogously, let us turn our attention to the simple models (the connections). In the class of models treated in the present work we always have $N_c = 2$ for any simple model $\mathcal{C}_c$ (a generalization could be in order, but we stick to the simplest case for the sake of clarity). Then we have three possibilities $(N_c^P, N_c^Q) = (1,1)$, $(N_c^P, N_c^Q) = (2,0)$, and $(N_c^P, N_c^Q) = (0,2)$. Particularly, in an iterative setting the latter case suffers from the same ill-posedness as the complex model with $N_n^P = 0$. For a simple model $\mathcal{C}_c$ we can write, from problem (2.6), the following relation (for the case where $(N_c^P, N_c^Q) = (1,1)$):

$$\begin{bmatrix} P_{\mathcal{C}_c,1} \\ Q_{\mathcal{C}_c,2} \end{bmatrix} = \mathcal{G}_{\mathcal{C}_c}\left(\begin{bmatrix} Q_{\mathcal{C}_c,1} \\ P_{\mathcal{C}_c,2} \end{bmatrix} \right), \tag{3.10}$$

where, as with expression (3.1), there is a time dependence that was not given explicitly for ease of notation. Hence, the functional relation maps, at any time, $\mathbb{R}^2$ onto itself, that is,

$$\mathcal{G}_{\mathcal{C}_c} : \mathbb{R} \times \mathbb{R} \to \mathbb{R} \times \mathbb{R} \quad \forall\ t, \tag{3.11}$$

and it represents the following problem (assuming that neither of the two boundaries of this simple model is a network outlet):

$$\begin{cases} M_c \frac{dQ_{\mathcal{C}_c,1}}{dt} + K_c Q_{\mathcal{C}_c,1} - (P_{\mathcal{C}_c,2} - P_{\mathcal{C}_c,1}) - B_c = 0 & \text{in } \mathcal{C}_c, \\ Q_{\mathcal{C}_c,1} + Q_{\mathcal{C}_c,2} = 0 & \text{in } \mathcal{C}_c. \end{cases} \tag{3.12}$$

Proceeding as before we can rearrange the equation to recast it through an implicit operator $\mathcal{F}_{\mathcal{C}_c}$ as follows:

$$\mathcal{F}_{\mathcal{C}_c}\left(\begin{bmatrix} P_{\mathcal{C}_c,1} \\ P_{\mathcal{C}_c,2} \end{bmatrix}, \begin{bmatrix} Q_{\mathcal{C}_c,1} \\ \mathcal{Q}_{C_c,2} \end{bmatrix} \right) = \mathcal{F}_{\mathcal{C}_c}(\mathbf{P}_{C_c}, \mathbf{Q}_{C_c}) = 0. \tag{3.13}$$

Remark 5. Suppose that we have $(N_c^P, N_c^Q) = (2, 0)$ and that the data at hand is P_1 and P_2. Then, problem (3.10) becomes

$$\begin{bmatrix} Q_{\mathcal{C}_c,1} \\ Q_{\mathcal{C}_c,2} \end{bmatrix} = [\mathcal{G}_{\mathcal{C}_c}^{SP}]^{-1}\left(\begin{bmatrix} P_{\mathcal{C}_c,1} \\ P_{\mathcal{C}_c,2} \end{bmatrix} \right). \tag{3.14}$$

Solving (3.12) we find the explicit form of operator $[\mathcal{G}_{\mathcal{C}_c}^{SP}]^{-1}$, and (3.14) yields

$$\begin{aligned} \begin{bmatrix} Q_{\mathcal{C}_c,1} \\ Q_{\mathcal{C}_c,2} \end{bmatrix} = & \begin{pmatrix} -\frac{1}{M_c}\int_0^t e^{-\frac{K_c}{M_c}(t-\sigma)}(\cdot)\mathrm{d}\sigma & \frac{1}{M_c}\int_0^t e^{-\frac{K_c}{M_c}(t-\sigma)}(\cdot)\mathrm{d}\sigma \\ \frac{1}{M_c}\int_0^t e^{-\frac{K_c}{M_c}(t-\sigma)}(\cdot)\mathrm{d}\sigma & -\frac{1}{M_c}\int_0^t e^{-\frac{K_c}{M_c}(t-\sigma)}(\cdot)\mathrm{d}\sigma \end{pmatrix} \begin{bmatrix} P_{\mathcal{C}_c,1} \\ P_{\mathcal{C}_c,2} \end{bmatrix} \\ & + \begin{pmatrix} \frac{1}{M_c}\int_0^t B_c e^{-\frac{K_c}{M_c}(t-\sigma)}\mathrm{d}\sigma \\ -\frac{1}{M_c}\int_0^t B_c e^{-\frac{K_c}{M_c}(t-\sigma)}\mathrm{d}\sigma \end{pmatrix}. \end{aligned} \tag{3.15}$$

This problem is well posed because for $P_{\mathcal{C}_c,1}$ and $P_{\mathcal{C}_c,2}$ given, we are able to find the values of $Q_{\mathcal{C}_c,1}$ and $Q_{\mathcal{C}_c,2}$. Nevertheless, the operator matrix in (3.15) is not invertible. This brings us to the problem of imposing flow rate at both ends of this component. In fact, suppose we have $(N_c^P, N_c^Q) = (0, 2)$; the data at hand now is $Q_{\mathcal{C}_c,1}$ and $Q_{\mathcal{C}_c,2}$, and problem (3.10) becomes

$$\begin{bmatrix} P_{\mathcal{C}_c,1} \\ P_{\mathcal{C}_c,2} \end{bmatrix} = \mathcal{G}_{\mathcal{C}_c}^{SP}\left(\begin{bmatrix} Q_{\mathcal{C}_c,1} \\ Q_{\mathcal{C}_c,2} \end{bmatrix} \right). \tag{3.16}$$

This functional relation is well posed just when $Q_{\mathcal{C}_c,1} + Q_{\mathcal{C}_c,2} = 0$ and we fix one of the pressure values; otherwise the problem is ill posed. Clearly, when the global problem is well posed the operator $\mathcal{G}_{\mathcal{C}_c}^{SP}$ exists. This is an example of the restrictions presented above on the choice of boundary conditions (see Remark 4).

Finally, consider the case $(N_c^P, N_c^Q) = (1, 1)$; the data at hand is $Q_{\mathcal{C}_c,1}$ and $P_{\mathcal{C}_c,2}$, and problem (3.10) is written as

$$\begin{bmatrix} P_{\mathcal{C}_c,1} \\ Q_{\mathcal{C}_c,2} \end{bmatrix} = \mathcal{H}_{\mathcal{C}_c}\left(\begin{bmatrix} Q_{\mathcal{C}_c,1} \\ P_{\mathcal{C}_c,2} \end{bmatrix} \right). \tag{3.17}$$

The explicit form of this operator is given by

$$\begin{bmatrix} P_{\mathcal{C}_c,1} \\ Q_{\mathcal{C}_c,2} \end{bmatrix} = \begin{pmatrix} -M_c \frac{d(\cdot)}{dt} - K_c(\cdot) & 1 \\ -1 & 0 \end{pmatrix} \begin{bmatrix} Q_{\mathcal{C}_c,1} \\ P_{\mathcal{C}_c,2} \end{bmatrix} + \begin{pmatrix} B_c \\ 0 \end{pmatrix}. \tag{3.18}$$

The convenience of dealing with implicit operators as in expression (3.13) is evident when we want to switch the role of the variables between data and unknowns, provided that each local problem is well posed.

3.2. Multicomponent treatment. The way in which we treat separately a given complex model or a given simple model has already been explained. In this section we describe the formulation involving the interaction of many components, which corresponds to the coupled problem (2.6).

As a first step we group all the interface variables $\{P^i\}_{i=1}^{i_T}$ and $\{Q^i\}_{i=1}^{i_T}$, given in global numeration, in the vector quantities $\mathbf{P}$ and $\mathbf{Q}$, respectively, that is,

$$\mathbf{P} = \begin{bmatrix} P^1 \\ P^2 \\ \vdots \\ P^{i_T} \end{bmatrix}, \qquad \mathbf{Q} = \begin{bmatrix} Q^1 \\ Q^2 \\ \vdots \\ Q^{i_T} \end{bmatrix}. \tag{3.19}$$

Such global quantities are related to the local quantities of each complex model through a mapping $\mathbf{R}_{N_n}$ as follows:

$$\mathbf{P}_{N_n} = \mathbf{R}_{N_n}\mathbf{P}, \qquad \mathbf{Q}_{N_n} = \mathbf{R}_{N_n}\mathbf{Q}, \tag{3.20}$$

where

$$\mathbf{P}_{N_n} = \begin{bmatrix} P_{\mathcal{N}_n,1} \\ P_{\mathcal{N}_n,2} \\ \vdots \\ P_{\mathcal{N}_n,N_n} \end{bmatrix}, \qquad \mathbf{Q}_{N_n} = \begin{bmatrix} Q_{\mathcal{N}_n,1} \\ Q_{\mathcal{N}_n,2} \\ \vdots \\ Q_{\mathcal{N}_n,N_n} \end{bmatrix}. \tag{3.21}$$

Likewise, we give the counterpart relation, denoted by $\mathbf{R}_{C_c}$, with the local quantities of each simple model

$$\mathbf{P}_{N_c} = \mathbf{R}_{C_c}\mathbf{P}, \qquad \mathbf{Q}_{N_c} = \mathbf{R}_{C_c}\mathbf{Q}, \tag{3.22}$$

where

$$\mathbf{P}_{N_c} = \begin{bmatrix} P_{\mathcal{C}_c,1} \\ P_{\mathcal{C}_c,2} \end{bmatrix}, \qquad \mathbf{Q}_{N_c} = \begin{bmatrix} Q_{\mathcal{C}_c,1} \\ Q_{\mathcal{C}_c,2} \end{bmatrix}. \tag{3.23}$$

These mappings also satisfy

$$\mathbf{P} = \sum_{n=1}^{n_T} \mathbf{R}_{N_n}^T \mathbf{P}_{N_n}, \qquad \mathbf{Q} = \sum_{n=1}^{n_T} \mathbf{R}_{N_n}^T \mathbf{Q}_{N_n}, \tag{3.24}$$

$$\mathbf{P} = \sum_{c=1}^{c_T} \mathbf{R}_{C_c}^T \mathbf{P}_{N_c}, \qquad \mathbf{Q} = \sum_{c=1}^{c_T} \mathbf{R}_{C_c}^T \mathbf{Q}_{N_c}, \tag{3.25}$$

establishing a mapping between local and global numerations.

Remark 6. The linear mappings $\mathbf{R}_{N_n} : \mathbb{R}^{i_T} \to \mathbb{R}^{N_n}$ and $\mathbf{R}_{C_c} : \mathbb{R}^{i_T} \to \mathbb{R}^{N_c}$ (recall that $N_c = 2$) are, algebraically speaking, rectangular matrices whose entries are zeros and ones.

For each coupling interface we have two unknowns P^i and Q^i, and the equations are provided by the corresponding implicit operators (3.9) (complex models) and (3.13) (simple models), that is,

$$\begin{aligned} \mathcal{F}_{\mathcal{N}_n}(\mathbf{P}_{N_n}, \mathbf{Q}_{N_n}) &= 0, \qquad n = 1, \ldots, n_T, \\ \mathcal{F}_{\mathcal{C}_c}(\mathbf{P}_{C_c}, \mathbf{Q}_{C_c}) &= 0, \qquad c = 1, \ldots, c_T. \end{aligned} \tag{3.26}$$

Changing now to a global numeration of the variables we get

$$\begin{aligned} \mathcal{F}_{\mathcal{N}_n}(\mathbf{R}_{N_n}\mathbf{P}, \mathbf{R}_{N_n}\mathbf{Q}) &= 0, \qquad n = 1, \ldots, n_T, \\ \mathcal{F}_{\mathcal{C}_c}(\mathbf{R}_{C_c}\mathbf{P}, \mathbf{R}_{C_c}\mathbf{Q}) &= 0, \qquad c = 1, \ldots, c_T. \end{aligned} \tag{3.27}$$

The next step consists in renumerating the interface equations using the transpose of the mappings $\mathbf{R}_{N_n}$ and $\mathbf{R}_{C_c}$, which implies

$$\begin{aligned} \mathbf{R}_{N_n}^T \mathcal{F}_{\mathcal{N}_n}(\mathbf{R}_{N_n}\mathbf{P}, \mathbf{R}_{N_n}\mathbf{Q}) &= 0, \qquad n = 1, \ldots, n_T, \\ \mathbf{R}_{C_c}^T \mathcal{F}_{\mathcal{C}_c}(\mathbf{R}_{C_c}\mathbf{P}, \mathbf{R}_{C_c}\mathbf{Q}) &= 0, \qquad c = 1, \ldots, c_T. \end{aligned} \tag{3.28}$$

With these sets of equations we assemble the global problem consisting of $2i_T$ interface unknowns

$$\begin{aligned} \mathcal{F}_{\mathcal{N}}(\mathbf{P}, \mathbf{Q}) &= \sum_{n=1}^{n_T} \mathbf{R}_{N_n}^T \mathcal{F}_{\mathcal{N}_n}(\mathbf{R}_{N_n}\mathbf{P}, \mathbf{R}_{N_n}\mathbf{Q}) = 0, \\ \mathcal{F}_{\mathcal{C}}(\mathbf{P}, \mathbf{Q}) &= \sum_{c=1}^{c_T} \mathbf{R}_{C_c}^T \mathcal{F}_{\mathcal{C}_c}(\mathbf{R}_{C_c}\mathbf{P}, \mathbf{R}_{C_c}\mathbf{Q}) = 0. \end{aligned} \tag{3.29}$$

This is the system of nonlinear interface equations associated to the coupled problem (2.6).

In some particular cases, from (3.29) it is possible to obtain the explicit relation between $\mathbf{P}$ and $\mathbf{Q}$ for components $\mathcal{N}$ and $\mathcal{C}$ yielding

$$\mathbf{P} = \mathcal{G}_{\mathcal{N}}^{SP}(\mathbf{Q}) \quad \text{or} \quad \mathbf{Q} = [\mathcal{G}_{\mathcal{N}}^{SP}]^{-1}(\mathbf{P}), \tag{3.30}$$

$$\mathbf{P} = \mathcal{G}_{\mathcal{C}}^{SP}(\mathbf{Q}) \quad \text{or} \quad \mathbf{Q} = [\mathcal{G}_{\mathcal{C}}^{SP}]^{-1}(\mathbf{P}). \tag{3.31}$$

Remark 7. In the classical domain decomposition context, usually the number of unknowns is reduced by making use of the Steklov–Poincaré mappings $\mathcal{G}_{\mathcal{N}}^{SP}$ and $\mathcal{G}_{\mathcal{C}}^{SP}$

whenever these operators exist (in the case of compliant pipes this is true; for rigid pipes see Remark 5). Indeed, after assembling the equations of all the complex models we attain the system of i_T nonlinear equations

$$\mathcal{T}_{\mathcal{N}}(\mathbf{Q}) = \sum_{n=1}^{n_T} \mathbf{R}_{N_n}^T \mathcal{F}_{\mathcal{N}_n}(\mathbf{R}_{N_n}\mathcal{G}_{\mathcal{C}}^{SP}(\mathbf{Q}), \mathbf{R}_{N_n}\mathbf{Q}) = 0, \tag{3.32}$$

or, performing the elimination in a different way,

$$\mathcal{T}_{\mathcal{C}}(\mathbf{Q}) = \sum_{c=1}^{c_T} \mathbf{R}_{C_c}^T \mathcal{F}_{\mathcal{C}_c}(\mathbf{R}_{C_c}\mathcal{G}_{\mathcal{N}}^{SP}(\mathbf{Q}), \mathbf{R}_{C_c}\mathbf{Q}) = 0. \tag{3.33}$$

These equations are two alternatives of the version of the Steklov–Poincaré method for the case of dimensionally-heterogeneous models treated in this work.

Remark 8. Giving continuation to the previous remark, the number of unknowns is reduced again by making use of the inverse of the Steklov–Poincaré mappings, that is, $[\mathcal{G}_{\mathcal{N}}^{SP}]^{-1}$ and $[\mathcal{G}_{\mathcal{C}}^{SP}]^{-1}$ (see (3.30) and (3.31)). Thus, we reach a set of i_T nonlinear equations given by

$$\mathcal{U}_{\mathcal{N}}(\mathbf{P}) = \sum_{n=1}^{n_T} \mathbf{R}_{N_n}^T \mathcal{F}_{\mathcal{N}_n}(\mathbf{R}_{N_n}\mathbf{P}, \mathbf{R}_{N_n}[\mathcal{G}_{\mathcal{C}}^{SP}]^{-1}(\mathbf{P})) = 0, \tag{3.34}$$

or, proceeding analogously to the previous remark,

$$\mathcal{U}_{\mathcal{C}}(\mathbf{P}) = \sum_{c=1}^{c_T} \mathbf{R}_{C_c}^T \mathcal{F}_{\mathcal{C}_c}(\mathbf{R}_{C_c}\mathbf{P}, \mathbf{R}_{C_c}[\mathcal{G}_{\mathcal{N}}^{SP}]^{-1}(\mathbf{P})) = 0. \tag{3.35}$$

It can be noted that these two expressions are versions of the FETI method for the particular case of dimensionally-heterogeneous models dealt with in this work. As with the previous remark, for linear problems both expressions are equivalent.

Remark 9. The previous remark states one of the most important features of the methodology proposed in the present article. In fact, for the classical Steklov–Poincaré and FETI methods it is necessary to be able to define the mappings $\mathcal{G}_{\mathcal{N}}^{SP}$, $\mathcal{G}_{\mathcal{C}}^{SP}$ and their inverses $[\mathcal{G}_{\mathcal{N}}^{SP}]^{-1}$, $[\mathcal{G}_{\mathcal{C}}^{SP}]^{-1}$. This limits the application of those more classical methods in the cases where such operators cannot be defined.

3.3. An example to clarify notation. In order to exemplify the notation introduced so far, let us consider a specific example like the one shown in Figure 3.1. It is a closed network (the set $\mathcal{O}_o$ is empty), and we will consider that we impose the traction (Neumann data) to all coupling points in all complex and simple components. Then, for the problem to be well posed the pressure has to be fixed at any point in the network, for which we assume a reference pressure at interface $\mathcal{I}_1$. This example resembles a network that will be employed in section 4. The aim of this example is to provide all the elements introduced in the previous section to this specific scenario.

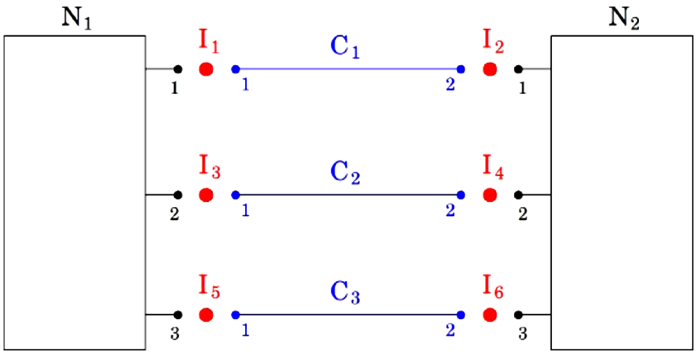

FIG. 3.1. *Specific network with* $i_T = 6$, $n_T = 2$, $c_T = 3$, *and* $o_T = 0$.

The matrices $\mathbf{R}_{N_n}$, $n = 1, 2$, and $\mathbf{R}_{C_c}$, $c = 1, 2, 3$, are given by

$$\mathbf{R}_{N_1} = \begin{pmatrix} 1 & 0 & 0 & 0 & 0 & 0 \\ 0 & 0 & 1 & 0 & 0 & 0 \\ 0 & 0 & 0 & 0 & 1 & 0 \end{pmatrix}, \qquad \mathbf{R}_{C_1} = \begin{pmatrix} 1 & 0 & 0 & 0 & 0 & 0 \\ 0 & 1 & 0 & 0 & 0 & 0 \end{pmatrix},$$

$$\mathbf{R}_{N_2} = \begin{pmatrix} 0 & 1 & 0 & 0 & 0 & 0 \\ 0 & 0 & 0 & 1 & 0 & 0 \\ 0 & 0 & 0 & 0 & 0 & 1 \end{pmatrix}, \qquad \mathbf{R}_{C_2} = \begin{pmatrix} 0 & 0 & 1 & 0 & 0 & 0 \\ 0 & 0 & 0 & 1 & 0 & 0 \end{pmatrix},$$

$$\mathbf{R}_{C_3} = \begin{pmatrix} 0 & 0 & 0 & 0 & 1 & 0 \\ 0 & 0 & 0 & 0 & 0 & 1 \end{pmatrix}.$$

Let us take for simplicity just the complex model $\mathcal{N}_1$. In this case, (3.26) for $n = 1$ reads

$$\mathcal{F}_{\mathcal{N}_1}(\mathbf{P}_{N_1}, \mathbf{Q}_{N_1}) = \begin{pmatrix} Q_{\mathcal{N}_1,1} - [\mathcal{G}^{SP}_{\mathcal{N}_1}]^{-1}_1(P_{\mathcal{N}_1,1}, P_{\mathcal{N}_1,2}, P_{\mathcal{N}_1,3}) \\ Q_{\mathcal{N}_1,2} - [\mathcal{G}^{SP}_{\mathcal{N}_1}]^{-1}_2(P_{\mathcal{N}_1,1}, P_{\mathcal{N}_1,2}, P_{\mathcal{N}_1,3}) \\ Q_{\mathcal{N}_1,3} - [\mathcal{G}^{SP}_{\mathcal{N}_1}]^{-1}_3(P_{\mathcal{N}_1,1}, P_{\mathcal{N}_1,2}, P_{\mathcal{N}_1,3}) \end{pmatrix} = \begin{pmatrix} 0 \\ 0 \\ 0 \end{pmatrix}, \tag{3.36}$$

where

$$[\mathcal{G}^{SP}_{\mathcal{N}_1}]^{-1} = \begin{pmatrix} [\mathcal{G}^{SP}_{\mathcal{N}_1}]^{-1}_1 \\ [\mathcal{G}^{SP}_{\mathcal{N}_1}]^{-1}_2 \\ [\mathcal{G}^{SP}_{\mathcal{N}_1}]^{-1}_3 \end{pmatrix}. \tag{3.37}$$

Then, expression (3.27) is

$$\mathcal{F}_{\mathcal{N}_1}(\mathbf{R}_{N_1}\mathbf{P}, \mathbf{R}_{N_1}\mathbf{Q}) = \begin{pmatrix} Q^1 - [\mathcal{G}^{SP}_{\mathcal{N}_1}]^{-1}_1(P^1, P^3, P^5) \\ Q^3 - [\mathcal{G}^{SP}_{\mathcal{N}_1}]^{-1}_2(P^1, P^3, P^5) \\ Q^5 - [\mathcal{G}^{SP}_{\mathcal{N}_1}]^{-1}_3(P^1, P^3, P^5) \end{pmatrix} = \begin{pmatrix} 0 \\ 0 \\ 0 \end{pmatrix}. \tag{3.38}$$

The application of the mapping $\mathbf{R}_{N_1}$ to $\mathcal{F}_{\mathcal{N}_1}$ yields the specific counterpart to (3.28), that is,

$$\mathbf{R}_{N_1}^T \mathcal{F}_{\mathcal{N}_1}(\mathbf{R}_{N_1}\mathbf{P}, \mathbf{R}_{N_1}\mathbf{Q}) = \begin{pmatrix} Q^1 - [\mathcal{G}^{SP}_{\mathcal{N}_1}]^{-1}_1(P^1, P^3, P^5) \\ 0 \\ Q^3 - [\mathcal{G}^{SP}_{\mathcal{N}_1}]^{-1}_2(P^1, P^3, P^5) \\ 0 \\ Q^5 - [\mathcal{G}^{SP}_{\mathcal{N}_1}]^{-1}_3(P^1, P^3, P^5) \\ 0 \end{pmatrix} = 0. \tag{3.39}$$

Performing the same steps for $\mathcal{N}_2$ we assemble the system of equations provided by the two complex models (see (3.29)) as follows:

$$\mathcal{F}_{\mathcal{N}}(\mathbf{P}, \mathbf{Q}) = \begin{pmatrix} Q^1 - [\mathcal{G}^{SP}_{\mathcal{N}_1}]^{-1}_1(P^1, P^3, P^5) \\ Q^2 - [\mathcal{G}^{SP}_{\mathcal{N}_2}]^{-1}_1(P^2, P^4, P^6) \\ Q^3 - [\mathcal{G}^{SP}_{\mathcal{N}_1}]^{-1}_2(P^1, P^3, P^5) \\ Q^4 - [\mathcal{G}^{SP}_{\mathcal{N}_2}]^{-1}_2(P^2, P^4, P^6) \\ Q^5 - [\mathcal{G}^{SP}_{\mathcal{N}_1}]^{-1}_3(P^1, P^3, P^5) \\ Q^6 - [\mathcal{G}^{SP}_{\mathcal{N}_2}]^{-1}_3(P^2, P^4, P^6) \end{pmatrix} = 0. \tag{3.40}$$

Analogously for the simple components after the assembling process we have

$$\mathcal{F}_{\mathcal{C}}(\mathbf{P}, \mathbf{Q}) = \begin{pmatrix} Q^1 - [\mathcal{G}^{SP}_{\mathcal{C}_1}]^{-1}_1(P^1, P^2) \\ Q^2 - [\mathcal{G}^{SP}_{\mathcal{C}_1}]^{-1}_2(P^1, P^2) \\ Q^3 - [\mathcal{G}^{SP}_{\mathcal{C}_2}]^{-1}_1(P^3, P^4) \\ Q^4 - [\mathcal{G}^{SP}_{\mathcal{C}_2}]^{-1}_2(P^3, P^4) \\ Q^5 - [\mathcal{G}^{SP}_{\mathcal{C}_3}]^{-1}_1(P^5, P^6) \\ Q^6 - [\mathcal{G}^{SP}_{\mathcal{C}_3}]^{-1}_2(P^5, P^6) \end{pmatrix} = 0, \tag{3.41}$$

where, for $c = 1, 2$, it is

$$[\mathcal{G}^{SP}_{\mathcal{C}_c}]^{-1} = \begin{pmatrix} [\mathcal{G}^{SP}_{\mathcal{C}_c}]^{-1}_1 \\ [\mathcal{G}^{SP}_{\mathcal{C}_c}]^{-1}_2 \end{pmatrix}. \tag{3.42}$$

Therefore, to obtain the solution $(\mathbf{P}, \mathbf{Q})$ we have to solve the system of nonlinear equations composed by (3.40) and (3.41) using any iterative method.

3.4. Coupling strategy in linear problems. In this section the strategy to be applied to deal with linear problems is outlined. For a more detailed presentation of this simpler case, the reader is referred to [15].

When all the submodels (complex and simple ones) are linear, the implicit functions $\mathcal{F}_{\mathcal{N}_n}$ and $\mathcal{F}_{\mathcal{C}_c}$ are affine relations. Then, the system of equations (3.29) can be rewritten in matricial form as

$$\begin{pmatrix} \mathsf{K}_{\mathbf{PP}} & \mathsf{K}_{\mathbf{PQ}} \\ \mathsf{K}_{\mathbf{QP}} & \mathsf{K}_{\mathbf{QQ}} \end{pmatrix} \begin{pmatrix} \mathbf{P} \\ \mathbf{Q} \end{pmatrix} = \begin{pmatrix} \mathsf{b}_{\mathbf{P}} \\ \mathsf{b}_{\mathbf{Q}} \end{pmatrix} \tag{3.43}$$

with

$$\mathsf{K}_{\mathbf{PP}} = \sum_{n=1}^{n_T} \mathbf{R}_{N_n}^T \mathbf{A}_{\mathcal{N}_n} \mathbf{R}_{N_n}, \tag{3.44}$$

$$\mathsf{K}_{\mathbf{PQ}} = \sum_{n=1}^{n_T} \mathbf{R}_{N_n}^T \mathbf{B}_{\mathcal{N}_n} \mathbf{R}_{N_n}, \tag{3.45}$$

$$\mathsf{K}_{\mathbf{QP}} = \sum_{c=1}^{c_T} \mathbf{R}_{C_c}^T \mathbf{A}_{\mathcal{C}_c} \mathbf{R}_{C_c}, \tag{3.46}$$

$$\mathsf{K}_{\mathbf{QQ}} = \sum_{c=1}^{c_T} \mathbf{R}_{C_c}^T \mathbf{B}_{\mathcal{C}_c} \mathbf{R}_{C_c}, \tag{3.47}$$

$$\mathsf{b}_{\mathbf{P}} = \sum_{n=1}^{n_T} \mathbf{R}_{N_n}^T \mathbf{Z}_{\mathcal{N}_n}, \tag{3.48}$$

$$\mathsf{b}_{\mathbf{Q}} = \sum_{c=1}^{c_T} \mathbf{R}_{C_c}^T \mathbf{Z}_{\mathcal{C}_c}, \tag{3.49}$$

where block matrices $\mathbf{A}_{\mathcal{N}_n}$, $\mathbf{A}_{\mathcal{C}_c}$, $\mathbf{B}_{\mathcal{N}_n}$, and $\mathbf{B}_{\mathcal{C}_c}$ above are the derivatives of the affine mappings $\mathcal{F}_{\mathcal{N}_n}$ and $\mathcal{F}_{\mathcal{C}_c}$ with respect to $\mathbf{P}$ and $\mathbf{Q}$, respectively, and block vectors $\mathbf{Z}_{\mathcal{N}_n}$ and $\mathbf{Z}_{\mathcal{C}_c}$ are the contributions of such mappings to the right-hand side.

As shown in [15], the system of equations (3.43) can be solved using any matrix-free version of any iterative method, without the need of assembling the system explicitly.

Remark 10. The system of equations (3.43) resembles the classical finite element assembling process if each component in the system is understood as, say, a very special generalized finite element. Therefore, we have that each $\mathcal{C}_c$, $c = 1, \ldots, c_T$, is a 0D finite element with four unknowns (two per coupling interface) and also that each $\mathcal{N}_n$, $n = 1, \ldots, n_T$, is a 3D finite element with twice as many unknowns as coupling interfaces (two unknowns per coupling interface). To summarize, their contributions to the interface equations are equivalent to the element contributions to node equations encountered in the assembling procedure of a finite element method.

3.5. Coupling strategy in nonlinear problems. When the problem is nonlinear, the system of equations (3.29) can be solved using any iterative method for solving systems of nonlinear equations. The main difficulty is that, except for very specific cases, the Jacobian of the system cannot be evaluated exactly, and the numerical evaluation becomes something computationally unaffordable. As a result, we must resort to a Jacobian-free iterative procedure for nonlinear systems of equations. In the present work, we shall analyze two of them: the so-called Broyden-update method (or simply Broyden) and the Newton-GMRES method (see [13]). These algorithms are presented in Table 3.1. Furthermore, two versions of the Broyden method are considered, the plain algorithm and an orthonormalized version.

In the descriptions of Broyden and Newton-GMRES algorithms given by Table 3.1 the stopping criterion is not detailed. In the actual implementation a (standard) stopping criterion is, of course, incorporated.

TABLE 3.1
Orthonormalized Broyden-update and Newton-GMRES algorithms for nonlinear systems.

System of m nonlinear equations of the form $F(x) = 0$	
Orthonormalized Broyden-update algorithm	Newton-GMRES algorithm
Given x_0 and B_0, compute $r_0 = F(x_0)$ **For j = 0 to m** $w_j = -B_j^{-1} r_j$ $v = w_j$ **For i = 0 to j − 1** $v = v - (v^T w_i) w_i$ **Enddo** $v = \frac{v}{\|v\|}$ $x_{j+1} = x_j + w_j$ $r_{j+1} = F(x_{j+1})$ $B_{j+1} = B_j + \frac{r_{j+1} v^T}{v^T w_j}$ **Enddo**	Given x_0, compute $r_0 = F(x_0)$ $v_1 = \frac{r_0}{\|r_0\|}$ **For j = 1 to m** $w_j = \frac{1}{\sigma}[F(x_0) - F(x_0 + \sigma v_j)]$ **For i = 1 to j** $h_{i,j} = w_j^T v_i$ $w_j = w_j - h_{i,j} v_i$ **Enddo** $h_{j+1,j} = \|w_j\|$ $v_{j+1} = \frac{w_j}{h_{j+1,j}}$ **Enddo** $x_m = x_0 + V_m H_m^{-1} \|r_0\| e_1$

In the Broyden method, when the inner loop is carried out, the algorithm is referred to as the orthonormalized version of the Broyden method. If this loop and the subsequent normalization are skipped, we refer to it simply as the Broyden method.

The main difference between the Broyden and Newton-GMRES methods is that the first method provides an estimate of the Jacobian of the system, which implies storing a $2i_T \times 2i_T$ matrix. In turn, the second method does not perform such an estimate (it is "matrix-free"). Moreover, while the orthonormalized version of the Broyden mtehod and the Newton-GMRES method converge to the exact solution, in the case of linear problems (with exact arithmetic), in $2i_T$ iterations, the plain Broyden method converges in $4i_T$ iterations. Although the matrix storage might be considered a disadvantage of the Broyden algorithm, it becomes something very desirable for transient problems. It is easy to show that the initialization matrix of these algorithms is equivalent to a preconditioner (see [13]). Therefore, for transient nonlinear problems, the number of iterations to reach the convergence can be reduced drastically by picking, as the initialization matrix, the estimation of the Jacobian obtained in the previous time step.

As well, the popular Gauss–Seidel method—with and without relaxation—and the pure Newton method—Jacobian calculated by finite differences—are considered in some comparisons.

4. Numerical results.

4.1. Implementation issues. Throughout the iterative process the 0D and 3D subproblems have to be solved. This implies performing the time discretization of the ordinary differential equation associated to the 0D model and the time and spatial discretizations of the 3D model.

For the 0D model a first order backward Euler method is employed, and the equation is treated in a fully implicit fashion. The time discretization in the 3D model is also accounted for by a first order backward Euler. The spatial discretization is carried out with the finite element method for the monolithic velocity-pressure problem. We make use of equal order interpolation with SUPG/PGP stabilization (see [7] for the details). For the Navier–Stokes component we employ the full symmetric gradient variational form, consistent with physical traction boundary conditions. Since each component

may have a nonlinear response (the Navier–Stokes equations indeed have), a linearization procedure must be taken into account when assessing the residual at each interation of the nonlinear solver of the coupling interface equations. In this work (unless stated otherwise) a Newton method is considered for the linearization of each nonlinear component. This gives rise to outer and inner iterations. The outer iterations are the iterations of the nonlinear solver for the system of coupling interface equations (Broyden, Gauss–Seidel, etc.), whereas the inner iterations are the iterations needed to evaluate the residual in the nonlinear components (Newton, fixed point, etc.). Regarding nonlinear tolerances, in all cases studied here (unless stated otherwise), convergence is achieved when the relative residual is less than $1 \cdot 10^{-6}$ or when the absolute residual is less than $1 \cdot 10^{-10}$.

Concerning the Broyden solver, unless stated otherwise we initialize the algorithm at the initial time step with the identity matrix, which is the worst-case scenario.

In all the examples presented below, the notation introduced in sections 2 and 3 can easily be identified, and no further reference is made. Finally, the units used in the examples follow the SI system.

4.2. On the boundary conditions at coupling interfaces. As aforementioned, when splitting an original dimensionally-heterogeneous system into dimensionally-homogeneous subsystems (stand-alone 0D/1D or 3D/2D problems), it is necessary to specify the way in which the coupling interface is going to behave for each one of these components. From the practical point of view we have some convenient choices.

- In the case of 0D noncompliant models we have the restriction stated in Remark 5 due to which we are not able to impose flow rate conditions on both ends of a given 0D model.
- In the case of 2D/3D models notice that it is far easier to impose a Neumann boundary condition, that is, to impose the normal traction, than to impose the flow rate, and yet in the latter case we have the issue from Remark 4.

In view of these comments, in all the examples that follow the complex models (2D/3D models) are fed with Neumann boundary data through all the coupling interfaces, while for the 0D models this is specified in each case.

The imposition of the flow rate in 2D/3D models, although more difficult than Neumann boundary conditions, can be performed (see [9], [11], [20], [21]). In any case, it is important to note that the flexibility in the choice of the boundary conditions permits us to formulate the problem making use of any available black-box solver (which may allow for flow rate and/or Neumann boundary conditions).

4.3. Example 1: Axisymmetric jet pump. This first example presents the simplest situation, in which we have one coupling interface. Then, the interface problem consists of two unknowns, namely, flow rate Q and normal force P. The problem dwells in modeling the flow produced by a jet pump in a reservoir through a secondary pipe, as shown in Figure 4.1. Particularly, we will model the jet flow produced in such a pipe of the reservoir. According to the spatial dimensions and flow regime, this pipe will be considered through a 2D axis-symmetric domain. The rightmost boundary in the domain of analysis is a traction-free boundary. Over the lower-left part, where the 2D model will be coupled to the 0D model (line C), a Neumann boundary condition is imposed. Also, a nonslip boundary condition is taken over the pipe wall, whereas for the rest of the boundary traction-free boundary conditions are assumed.

In Figure 4.2 the dimensions are specified. According to the notation of this figure we have $Z = 0.9$ m, $h = 0.1$ m, $H = 0.3$ m, and $W = 6.3$ m. In addition, all the

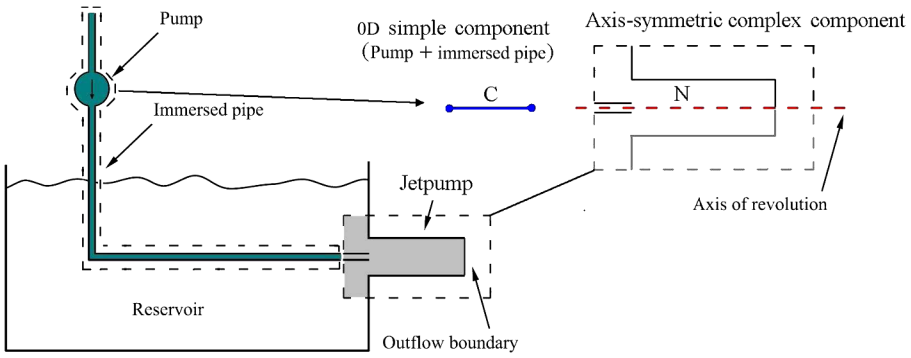

FIG. 4.1. *Reservoir with a jet pump.*

boundary conditions are given. The immersed pipe with the pump is incorporated in the problem through a 0D model, which is coupled with the 2D axis-symmetric model for the pipe through the lower-left interface (thick line; see Figure 4.2). This coupling interface is such that we impose the flow rate to the 0D model and the pressure—coupling force—(a Neumann boundary condition) to the 2D model.

For this problem we simulate the effect of an oscillatory pump characterized by its mean value P_{mean}, the mean-to-maximum oscilation amplitude P_{amp}, and the period T. These data are specified in each case. The density and viscosity of the fluid are $\rho = 1$ kg/m^3 and $\mu = 0.01$ Pa.s, respectively. Recall that the parameters that characterize the 0D model corresponding to the immersed pipe are $L = 6$ m (unless stated otherwise) and $R = h$; therefore, $A = \pi h^2$ for the 0D model. The time step in all tested cases was $\Delta t = 0.05$ s, and the spatial discretization resulted in a 2D mesh with 7265 nodes.

We choose this simple situation to carry out the sensitivity analysis of the number of iterations to achieve convergence with respect to different elements in the problem: (1) the iterative algorithm used to solve the interface problem, (2) the qualitative and quantitative form of the pump signal, and (3) the parameters that define the 0D pipe.

4.3.1. Sensitivity with respect to the iterative algorithm. First of all we compare different iterative algorithms when imposing a squared wave at the entrance of the pipe defined by $P_{\text{mean}} = 300$ Pa, $P_{\text{amp}} = 30$ Pa, and $T = 1$ s. In Figure 4.3 the solution at the coupling interface (flow rate and normal force) is presented together with the comparison of the performance of the different methods: orthonormalized Broyden

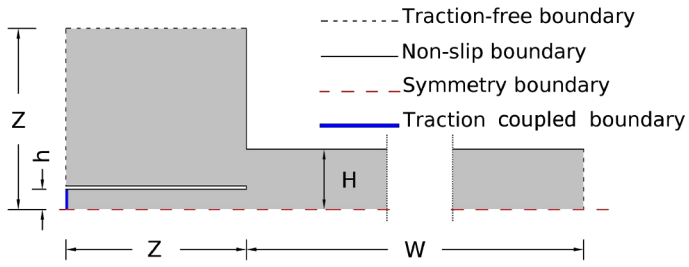

FIG. 4.2. *Details of the axis-symmetric geometry of the complex component.*

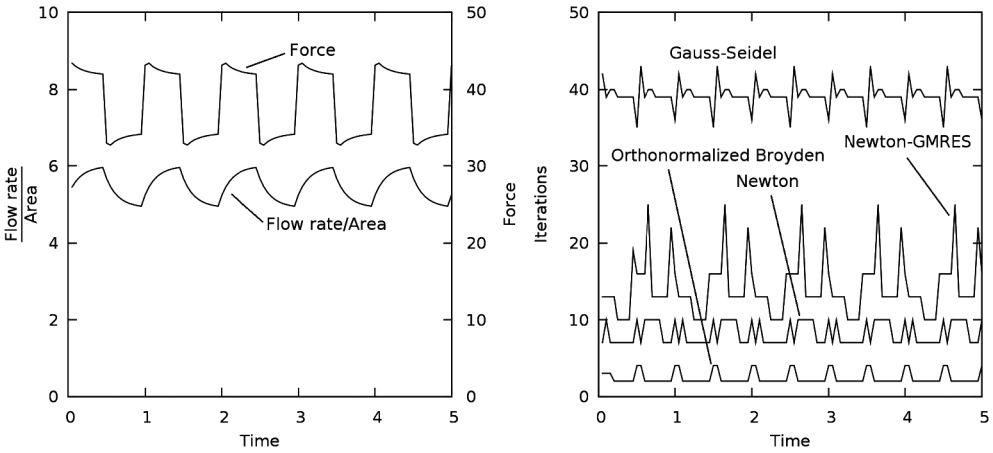

FIG. 4.3. *Performance of different iterative algorithms for the square waveform.*

method and Newton-GMRES method (see Table 3.1) and Gauss–Seidel and pure Newton methods.

We observe that the Broyden method performs much better than the other methods. In particular, we note the poor convergence properties of the Newton-GMRES method. Even the pure Newton method takes fewer iterations to converge. The worst case is the Gauss–Seidel solver as expected (relaxation $\omega = 0.25$). Also, numerical tests were carried out taking $P_{\text{mean}} \in \{100 \text{ Pa}, 200 \text{ Pa}\}$, rendering analogous results (not presented here) in terms of the number of iterations performed by each method, exhibiting an apparent lack of sensitivity with respect to the Reynolds number.

4.3.2. Sensitivity with respect to the pump waveform. In order to gain insight into the performance of the methods, we investigate the sensitivity of the number of iterations with respect to the waveform applied through the 0D pipe. Here we focus on the Broyden method, and we employ three kinds of signals: (i) sine, (ii) tooth, and (iii) square. The period is $T = 1$ s, $P_{\text{mean}} = 300$ Pa, and $P_{\text{amp}} = 30$ Pa. Figure 4.4

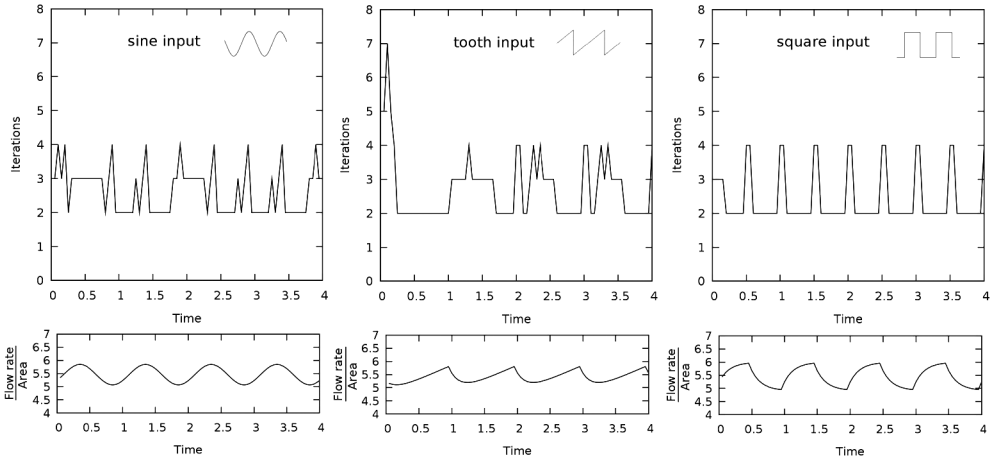

FIG. 4.4. *Performance of orthonormalized Broyden method for different input conditions.*

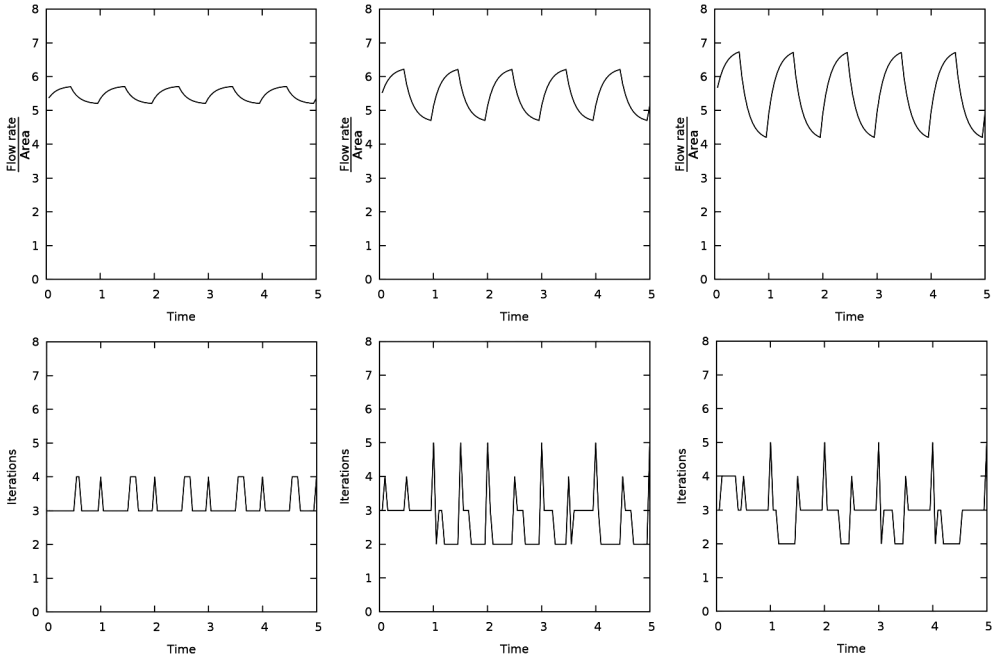

FIG. 4.5. *Performance of orthonormalized Broyden method for different amplitudes of the square wave.*

features the number of iterations for the three input conditions. As well, the flow rate at the coupling interface is given. It can be noticed that there are no significant differences when changing the forcing pump regarding the average number of iterations to achieve convergence.

In addition, we close this example testing for the square waveform and for the same $P_{\text{mean}} = 300$ Pa and $T = 1$ s, different amplitudes $P_{\text{amp}} \in \{15 \text{ Pa}, 45 \text{ Pa}, 75 \text{ Pa}\}$. Figure 4.5 displays the resulting flow rate at the coupling point, and the performance of the Broyden method is assessed. Note that although the amplitude enlarges significantly, the number of interations taken to achieve convergence changes slightly.

Finally, we modify the frequency that defines the square signal in the pump in order to evaluate the robustness of the Broyden method, which appears to be the best method according to the previous findings. As well, we compare this performance with the Gauss–Seidel method. Thus we consider $P_{\text{mean}} = 300$ Pa, $P_{\text{amp}} = 30$ Pa, and a period ranging $T \in \{0.3 \text{ s}, 0.5 \text{ s}, 1.0 \text{ s}, 2.0 \text{ s}, 3.0 \text{ s}\}$. The results are summarized in Table 4.1. In this table the Broyden method is shown to be also insensitive to the frequency of the input signal (recall that the same time step was used in all cases, $\Delta t = 0.05$ s). As for the relaxed Gauss–Seidel method, the relaxation parameter was taken to be $\omega = 0.25$ which was tested to be among the ones that made the Gauss–Seidel method perform better for this case.

4.3.3. Sensitivity with respect to the physical parameters. In this section we test the behavior of the orthonormalized Broyden and Gauss–Seidel algorithms with respect to variations in the physical parameters. We focus on the length of the 0D pipe, denoted by L, which, in turn, changes the values of $M = \frac{\rho L}{A}$ and $K = \frac{8\pi\mu L}{A^2}$ according to the expression (2.2). The rest of the parameters are $P_{\text{mean}} = 300$ Pa, $P_{\text{amp}} = 30$ Pa, and

TABLE 4.1
Number of iterations for the different periods.

	Iterations (min-max)	
Period, T	Orthonormalized Broyden	Relaxed Gauss–Seidel ($\omega = 0.25$)
0.3	2–4	35–40
0.5	2–4	35–41
1.0	2–4	36–43
2.0	2–4	36–43
3.0	2–2	36–39

$T = 1$ s with $\Delta t = 0.05$ s. In Table 4.2, we present the iteration number for different values of L for the Broyden and Gauss–Seidel algorithms. In the last case we consider with ($\omega = 0.25$) and without ($\omega = 1.0$) relaxation.

We observe in Table 4.2 that the number of iterations for the Broyden algorithm is bounded to less than 10 in all range of values of L, while for Gauss–Seidel the number of iterations depends strongly on L and also on the chosen relaxation parameter ω. Hence, the Broyden method turns out to be far less expensive and robust than the Gauss–Seidel method.

4.4. Example 2: Interconnected closed system with two pumps. The aim of this second example is to analyze a more complex situation where the fluid is confined in a closed-loop network as shown in Figure 4.6. Two forcing pumps are introduced in the vertical pipes that drive the fluid through the pipes and the five fluid collector compartments. In the 2D fluid compartments all the boundaries, save for those in which we perform a coupling with a 0D model, are no-slip boundaries. The number of coupling interfaces is 16; therefore the number of unknowns in the interface problem is 32. When spliting the system into homogeneous subsystems we apply Neumann boundary conditions on the 2D models (the normal force) and pressure on the 0D models. Since the network is closed we fixed the pressure reference value ($P_{\text{ref}} = 0$).

As already said, there are two sinusoidal pumps with amplitudes $P_{1,\max} = P_{2,\max} = 150$ Pa and periods $T_1 = 10$ s and $T_2 = 7$ s, respectively. Index 1 denotes the pump located over the left vertical pipe and index 2 is used for the right vertical pipe. The

TABLE 4.2
Number of iterations for different values of L.

	Iterations (min-max)		
L	Orthonormalized Broyden	Relaxed Gauss–Seidel ($\omega = 0.25$)	Gauss–Seidel
0.12	3–5	49–49	7–8
0.6	3–5	46–49	23–24
1.2	3–10	37–49	diverges
6.0	2–4	36–43	diverges
12.0	7–7	diverges	diverges
60.0	2–4	diverges	diverges
120.0	2–2	diverges	diverges

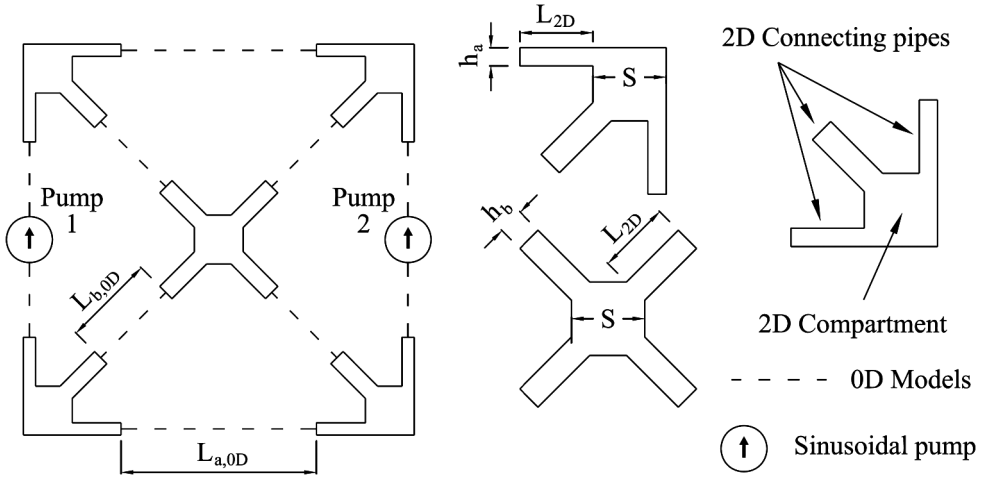

FIG. 4.6. *Closed-loop conduction system with two forcing pumps.*

density and viscosity of the fluid are $\rho = 1$ Kg/m^3 and $\mu = 0.01$ Pa.s, respectively. The 2D compartments are squares with a side measure $S = 4$ m. The 2D connecting pipes that are incoming and outgoing the compartments are all $L_{2D} = 4$ m long; the vertical and horizontal ones have a separation between the parallel plates $h_a = 1$ m, whereas for the diagonal pipes this separation is $h_b = \sqrt{2}$ m. In turn, the vertical and horizontal 0D models are configured such that they represent pipes (actually parallel plates) $L_{a,0D} = 16$ m long, while the diagonal 0D models are such that the pipes they represent are approximately $L_{b,0D} = 7.556$ m long so as to get the conduction system closed. The time step used was $\Delta t = 0.1$ s, and the spatial discretization rendered meshes of approximately 1100 nodes per 2D component. Throughout the simulation the Reynolds number reaches a maximum value of $\mathrm{Re}_{\max} \simeq 1100$.

Different iterative methods were tested in this case: (i) Broyden, (ii) Broyden with orthonormalization, and (iii) Newton-GMRES with parabolic line search. In Figure 4.7 a comparison of the performance of the different nonlinear solvers is presented. From the figure we conclude that the Broyden method with orthonormalization is without a doubt the best option, taking 4 to 6 iterations per time step to converge. The pure Broyden method is less effective than its orthonormalized version, taking between 20 and 30 iterations. Nevertheless, both versions of the Broyden algorithm are more convenient than the Newton-GMRES algorithm, which takes around 30 iterations at each time step.

Recall that the Broyden method builds an inverse matrix that is an approximation of the Jacobian as time goes by. Thus, such a matrix is used at each time step to initialize the iterations (initialization of the approximate Jacobian). This is quite an interesting aspect of Broyden methods, in contrast with the Newton-GMRES method, for which, since it is a matrix-free method, no approximate Jacobian is built along the iterations. Hence, in this sense, the Broyden method must be seen as a preconditioned method, whereas the Newton-GMRES method is just initialized with the solution of the previous time step. Matrix-free preconditioning techniques for the Newton-GMRES method are out of the scope of the present paper but are worth exploring in future works.

The initialization using the exact Jacobian computed just once at the first time step is another option which improves the performance of both Broyden methods. Figure 4.8 gives a comparison between (i) the orthonormal Broyden with initialization, that is,

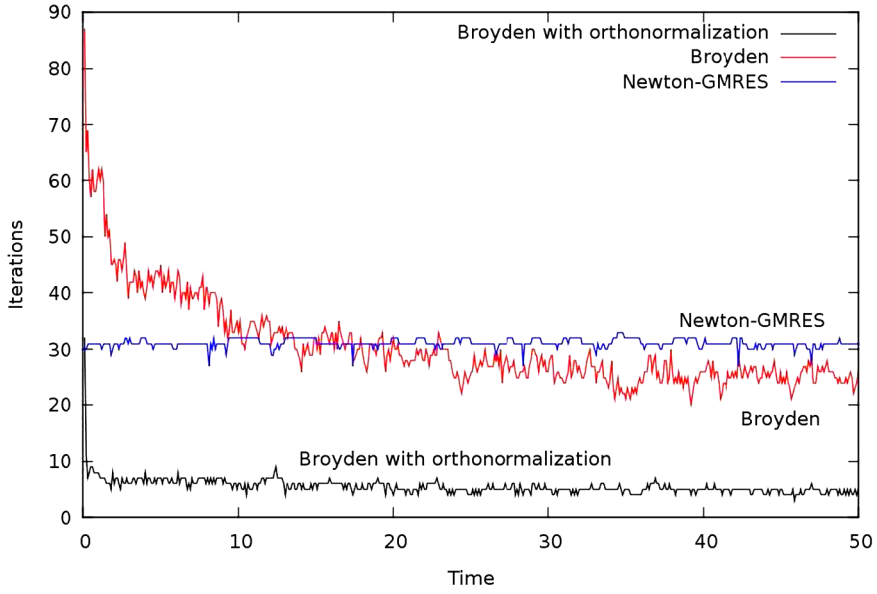

FIG. 4.7. *Performance of the different nonlinear solvers.*

using the Jacobian of the Newton method as initial matrix for the first time step, and (ii) the orthonormal Broyden case without initialization, that is, when the initial matrix is the identity. There it can be seen that the initialization improves the convergence properties of the Broyden method. The case of the Broyden method without orthonormalization exhibits the same behavior.

Figure 4.9 presents the flow rate as a function of time for each one of the 0D connecting elements. Also, the complexity of the system dynamics can be seen in this figure.

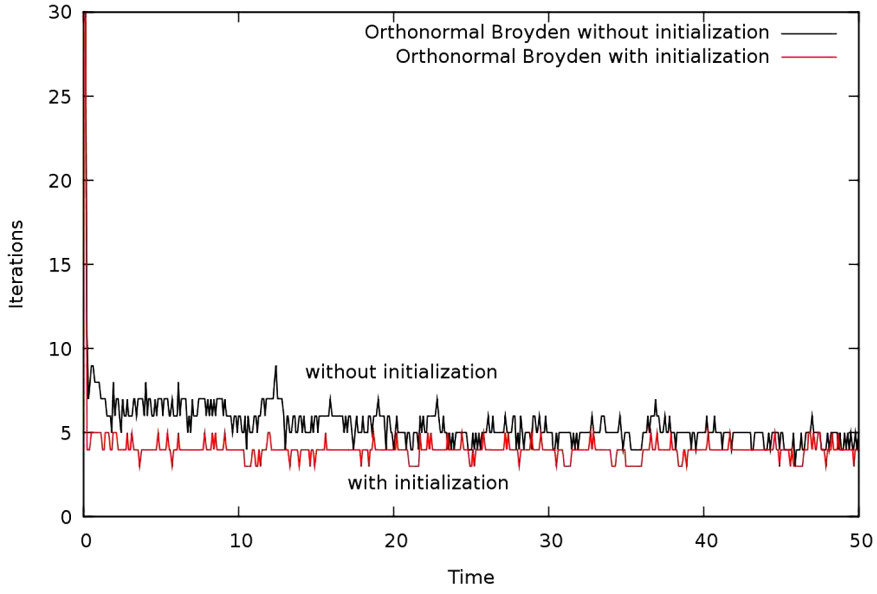

FIG. 4.8. *Orthonormal Broyden with and without Jacobian initialization.*

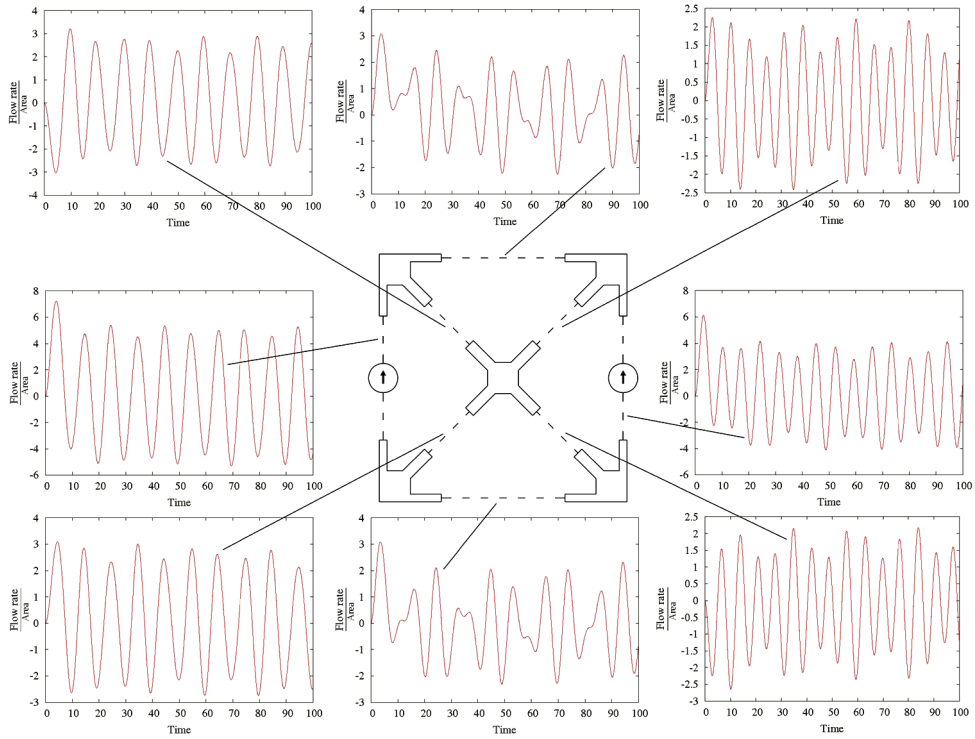

FIG. 4.9. *Flow rate over area at each* 0*D connecting element.*

For obvious reasons, we present the flow rate corresponding to each 0D model, which is the corresponding flow rate to the associated coupling interfaces at both sides of such a 0D model. The sign of the flow rate is consistent with the following definition: (i) for the four 0D pipes which surround the system (left, right, up, and down pipes), the flow rate is positive in the clockwise direction, and (ii) for the four 0D pipes which are linked to the center of the system, the flow rate is positive in the outward direction (going away from the center).

In turn, Figure 4.10 shows the velocity magnitude for different time instants in a given period of the whole simulation. In the sequence of figures the complex interactions among the 2D components can be appreciated. In this regard, in spite of the high level of coupling due to the fact that the system is closed, the Broyden algorithm with orthonormalization performs quite well.

4.5. Example 3: Closed parallel 3D system. The problem involves the flow of a fluid driven by a pump which connects two 3D collectors. Two other connectors are included in the system. All the connectors are modeled with 0D representations. The scheme is shown in Figure 4.11. In the 3D fluid collectors all the boundaries, except the coupling ones, are homogeneous Dirichlet boundaries (nonslip condition). Here we have 6 coupling interfaces; then the interface problem consists of 12 unknowns. As before, all coupling interfaces are Neumann boundaries concerning the 0D and 3D submodels, and the pressure is fixed to a reference value ($P_{\text{ref}} = 0$) because the network is closed.

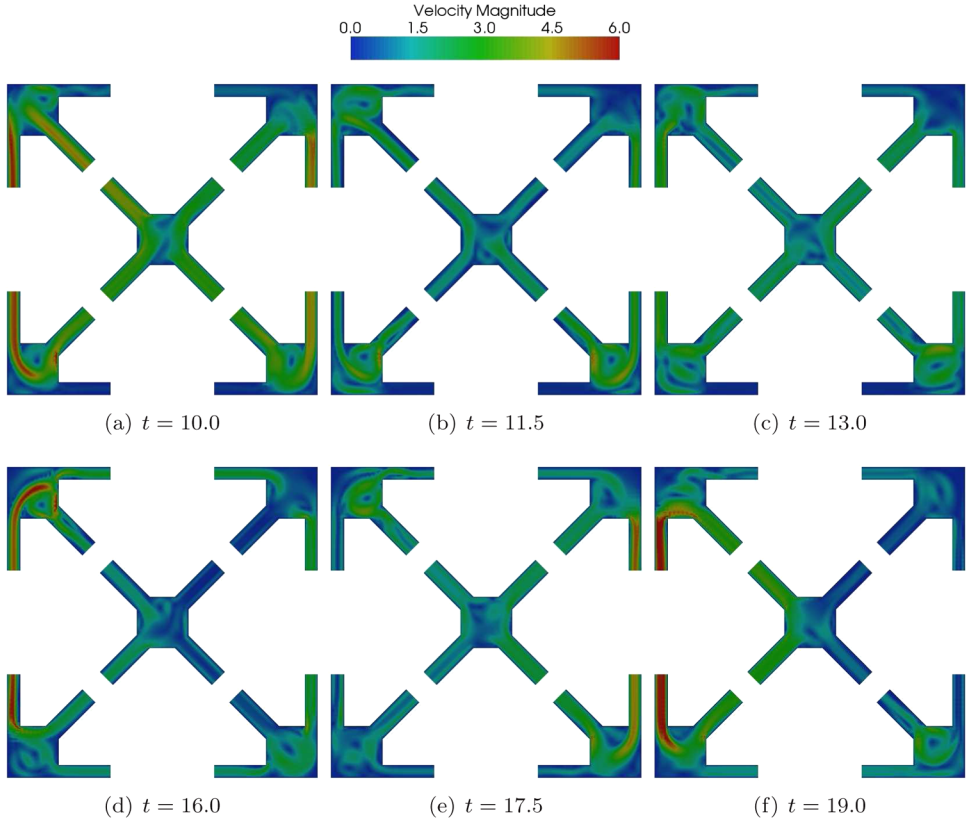

(a) $t = 10.0$ (b) $t = 11.5$ (c) $t = 13.0$

(d) $t = 16.0$ (e) $t = 17.5$ (f) $t = 19.0$

FIG. 4.10. *Velocity magnitude for different instants.*

Although the system is smaller than in the previous section, in this case the coupling level with respect to the number of unknowns coupled over each interface is more critical. Indeed, given a certain fixed number of coupling interfaces, and assuming a correspondence in the number of degrees of freedom over the coupling interfaces with the dimension of the problem, the monolithic approach for a 3D-0D problem is more expensive than the 2D-0D counterpart. In addition, the associated matrix of the linear counterpart of the interface problem is more dense.

The sinusoidal pump is defined by an amplitude $P_{\max} = 25$ Pa and period $T_1 = 10$ s. The density and viscosity of the fluid are, again, $\rho = 1$ kg/m^3 and $\mu = 0.01$ Pa.s, respectively. The 3D collectors are cylinders with three connections symmetrically distributed over one of the flat sides. The dimensions of the system, according to Figure 4.11, are $R_e = 3$ m, $R_i = 2$ m, $r = 0.5$ m, $H = 7$ m, and $h = 1$ m. The 0D connections are configured such that they represent the corresponding pipes with $L_{0D} = 16$ m long. The mesh of each collector is, approximately, of 7000 nodes, and the Reynolds number has a maximum value of $\mathrm{Re}_{\max} \simeq 100$ during the simulation.

In consideration of the results seen in the previous sections, here we restrict ourselves to the use of the Broyden method with orthonormalization for solving the nonlinear interface problem. In the present example we analyze how the convergence is affected when changing the time step in the simulation. Three time steps are used; they are (i) $\Delta t_1 = 0.025$ s, (ii) $\Delta t_2 = 0.05$ s, and (iii) $\Delta t_3 = 0.1$ s.

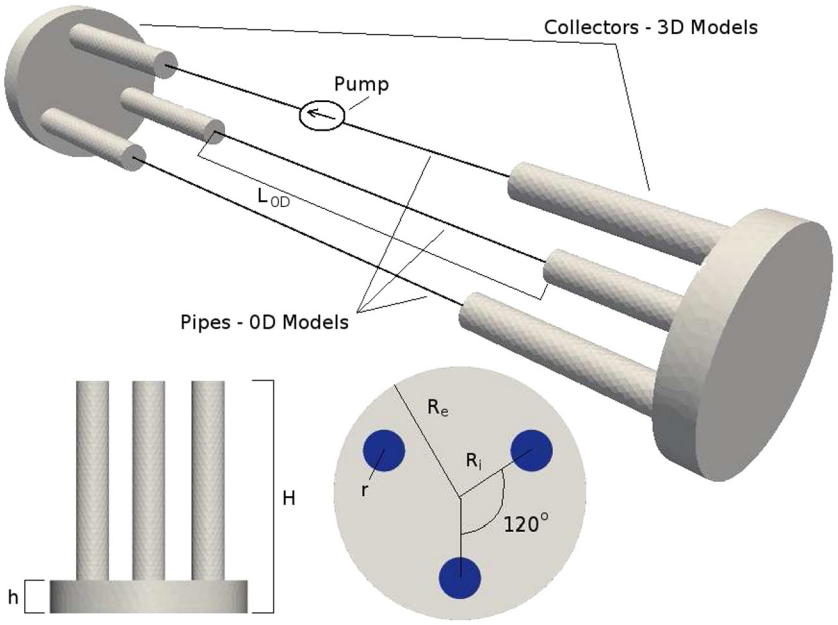

FIG. 4.11. *Closed-loop 3D conduction system with a forcing pump.*

In Figure 4.12 the results are presented with a comparison of the iterations needed to converge for the time steps tested. For the first time step, since the Broyden method is started from the identity matrix, it takes (i) 13, (ii) 13, and (iii) 15 iterations to converge. It was removed from the plots in Figure 4.12 so as to compare the details once the

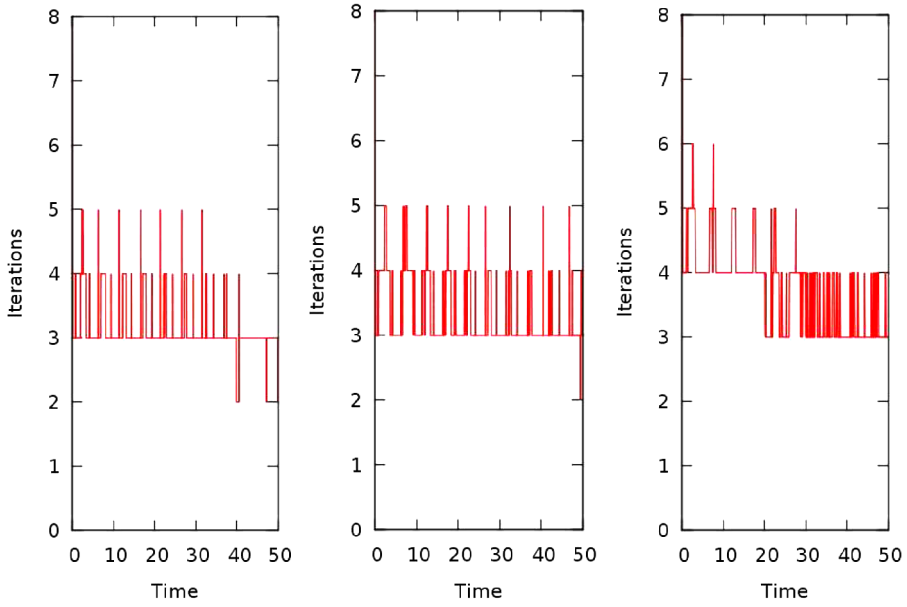

(a) $\Delta t = 0.025$ (b) $\Delta t = 0.05$ (c) $\Delta t = 0.1$

FIG. 4.12. *Performance of the orthonormalized Broyden method for different time steps.*

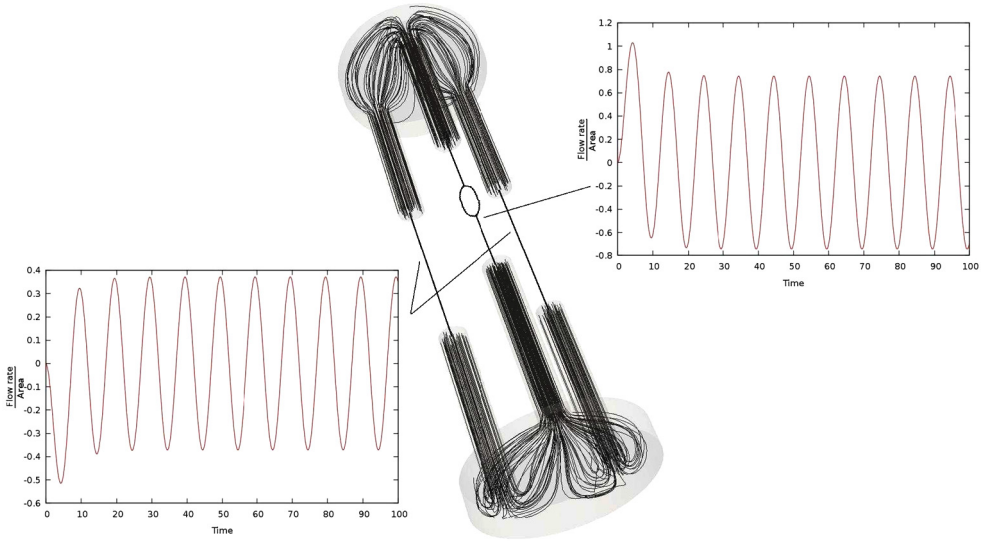

FIG. 4.13. *Flow rate versus time in the pipes and streamlines at* $t = 25$ s.

periodic regime is established. Notice that the convergence properties remain almost the same as the time step is increased.

Figure 4.13 presents the flow rate in the three pipes as a function of time. As well, the streamlines at time $t = 25$ s are plotted. Evidently, due to the symmetry of the system, the two inferior pipes in the figure behave in the same manner, whereas the superior pipe is the one that contains the pump and therefore drives the flow. In addition, to appreciate the dynamics of the system in Figure 4.14, a detail of the velocity field in different transversal cuts is displayed at four time instants along a certain cycle of the pressure pump.

4.6. Example 4: Blood flow in the arm. In this last section we present an application to hemodynamics, complementing a previous work on decomposition of 1D models [3]. We deal with the arterial network of the arm with slightly different physical components than before. The so-called simple components (or simple models) are 1D models for the flow of an incompressible fluid in compliant vessels, while the complex components (or complex models) are 3D Navier–Stokes equations in compliant domains (see [2], [19] for more details on these components). Therefore, the operators $\mathcal{G}_{\mathcal{N}_n}$ and $\mathcal{G}_{\mathcal{C}_c}$ for the complex and simple models, introduced in section 3 (see (3.4) and (3.10), respectively), correspond to the solution of these problems. The evaluation of the nonlinear components in this case is carried out using fixed point iterations (see again [2], [19] for more details about the numerical approximation).

The scheme of the coupled system can be seen in Figure 4.15. The 3D-1D model of the arm is set up starting from the subclavian artery and following the main branches found in the arm. It consists of a 1D model for which the five larger bifurcations have been replaced by 3D geometries. Also, an inflow boundary condition is prescribed, as shown in Figure 4.15, whereas at the outflow boundaries 3-element Windkessel models are considered. All the mechanical and geometrical properties are taken from the data given in [2]. The boundary condition is taken from a pure 1D model of the whole arterial tree. It is noticed that the interface problem consists of 15 coupling interfaces, and then 30 interface unknowns (flow rate and pressure). When splitting the network into 1D and

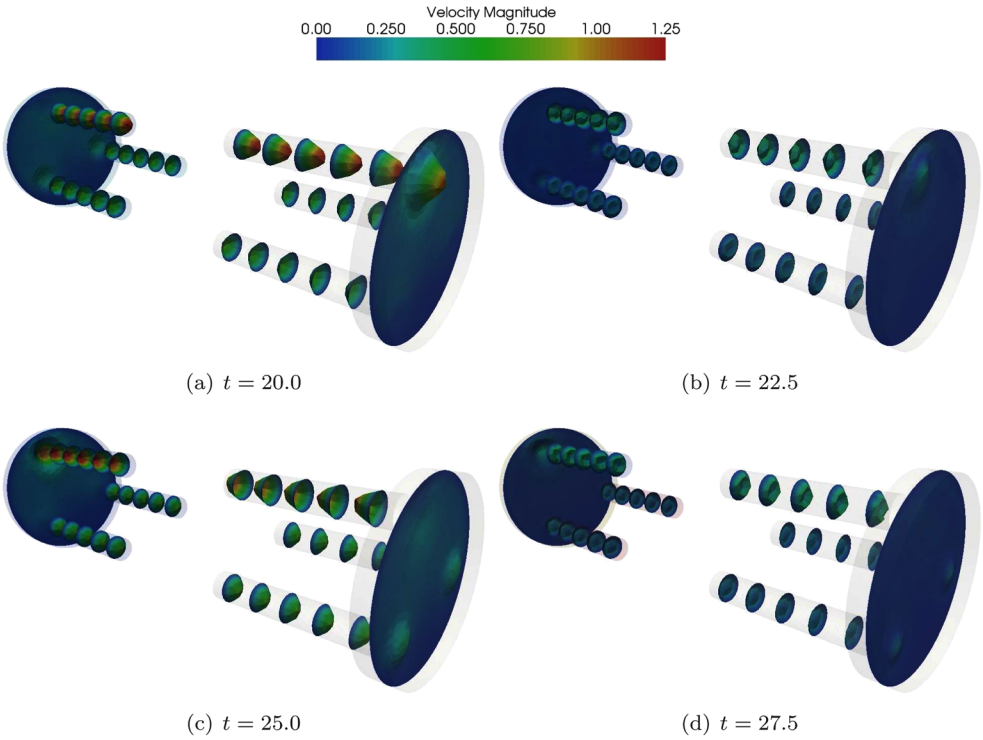

(a) $t = 20.0$ (b) $t = 22.5$

(c) $t = 25.0$ (d) $t = 27.5$

FIG. 4.14. *Warp of the velocity field for different time instants.*

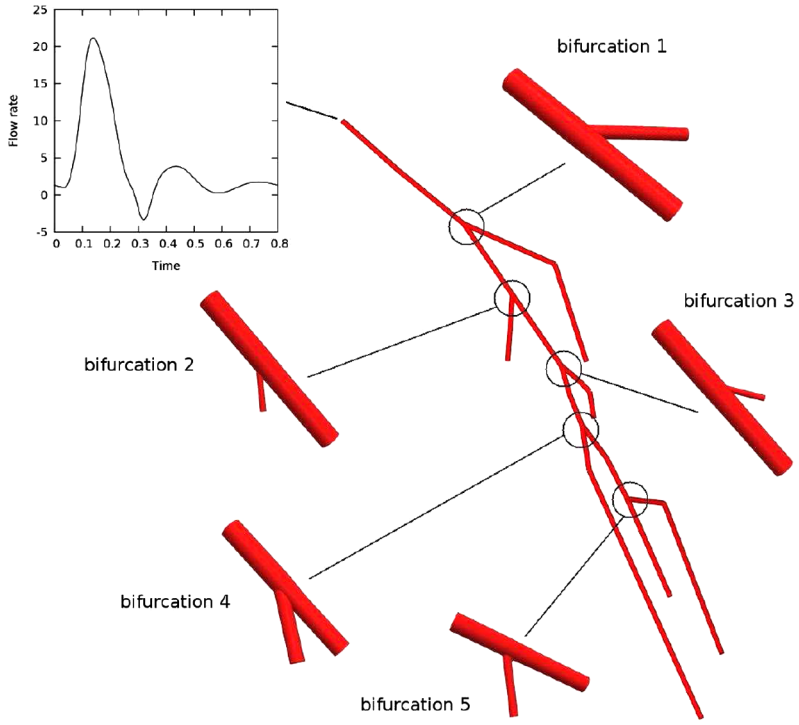

FIG. 4.15. *Coupled 3D-1D system to represent the arterial branches in the arm.*

3D models we have considered the coupling interfaces to behave as Neumann boundaries for all the components.

The convergence in this problem is considered when the relative residual is less than $1 \cdot 10^{-4}$, as well as when the absolute residual is less than $1 \cdot 10^{-8}$. The cardiac beat is characterized by a period of $T = 0.8$ s, while the time step, which is limited by convergence issues related to the 3D components, is $\Delta t = 6.25 \cdot 10^{-4}$ s. Three cardiac cycles have been simulated, and the results presented here correspond to the last cycle, when it can be considered that the periodic state has been established. The dimensional units are cm^3/s and $\mathrm{dyn}/\mathrm{cm}^2$ for flow rate and pressure, respectively. The discretization of the 3D models resulted in meshes of approximately 20000 nodes per 3D component. Based on our previous experience in the hemodynamics field (see [3] for more details) and also on the tests performed in the previous sections, we choose the Broyden method without orthonormalization to solve the interface problem, and at each cardiac beat the Broyden method is initialized with the Jacobian matrix (computed by finite differences).

The performance of the Broyden method is presented in Figure 4.16. There, the flow rates at each one of the inlets of the 3D models are also displayed. We point out that although the interface problem has 30 degrees of freedom, the Broyden method applied to the interface problem requires just between 3 and 10 iterations per time step to converge. This puts in evidence the robustness of the partitioning strategy developed here even in situations involving more sophisticated complex and simple components.

The results for the coupling unknowns at the interfaces among the 3D and 1D models are presented in Figure 4.17. There, the results (pressure and flow rate) at the inlet of each one of the five 3D bifurcations are displayed. In that figure, the propagation phenomenon can be noticed clearly as a result of the compliance of the models employed in the simulation.

Finally, the magnitude of the velocity field at several time instants throughout the cardiac cycle is featured in Figure 4.18. Though very simplified 3D geometries have been

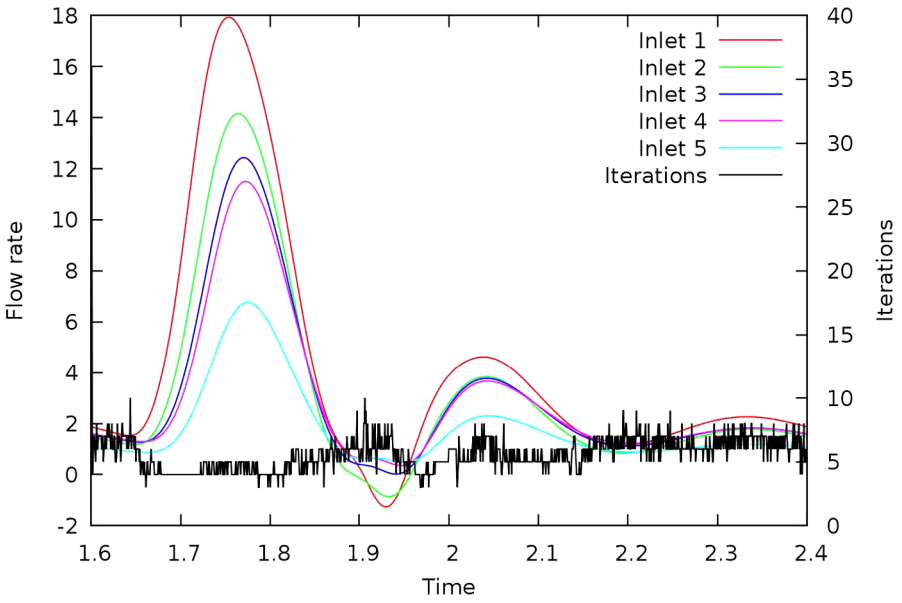

FIG. 4.16. *Performance of the Broyden method and flow rates at inlets of each bifurcation.*

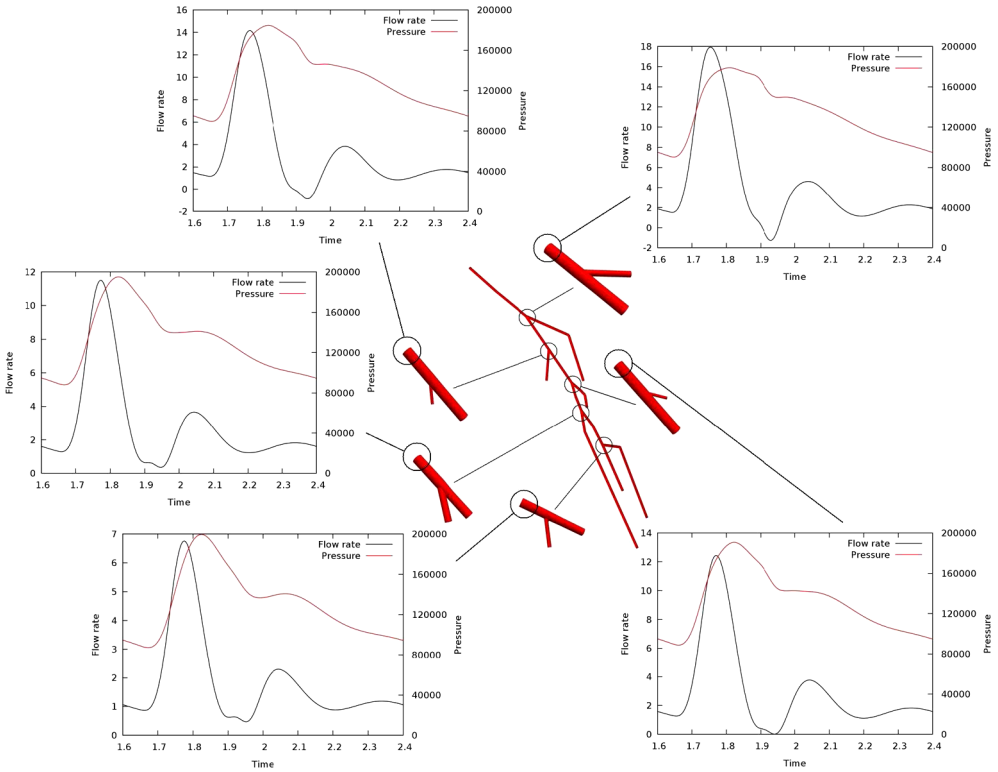

FIG. 4.17. *Flow rate and pressure at some coupling interfaces.*

adopted for the bifurcations in this example, the complexity of the blood flow is remarkable. Indeed, Womersley-like velocity profiles due to inverse pressure gradient and recirculation regions are observed around $t = 0.3$.

The use of the present methodology for dealing with the coupling of 1D models and patient-specific 3D geometries obtained from medical images is straightforward, not entailing further issues from the point of view of the convergence of the iterative methods proposed here.

5. Conclusions. In this work, a partitioning procedure for solving iteratively coupled dimensionally-heterogeneous models has been set up within the context of the numerical simulation of fluid mechanics problems. The methodology was developed by recasting the monolithic problem as a nonlinear problem written in terms of interface variables, those which perform the coupling. For the cases treated in this work these physical variables were flow rate and its dual variable (the normal component of the traction vector). Several nonlinear solvers have been compared in different situations, in which Broyden-like methods turn out to perform far better than the classical Gauss–Seidel method and even better than the Newton-GMRES algorithm. As well, the iterative strategy was tested in 2D and 3D problems, performing satisfactorily even in situations involving deforming domains like those encountered in the hemodynamics field.

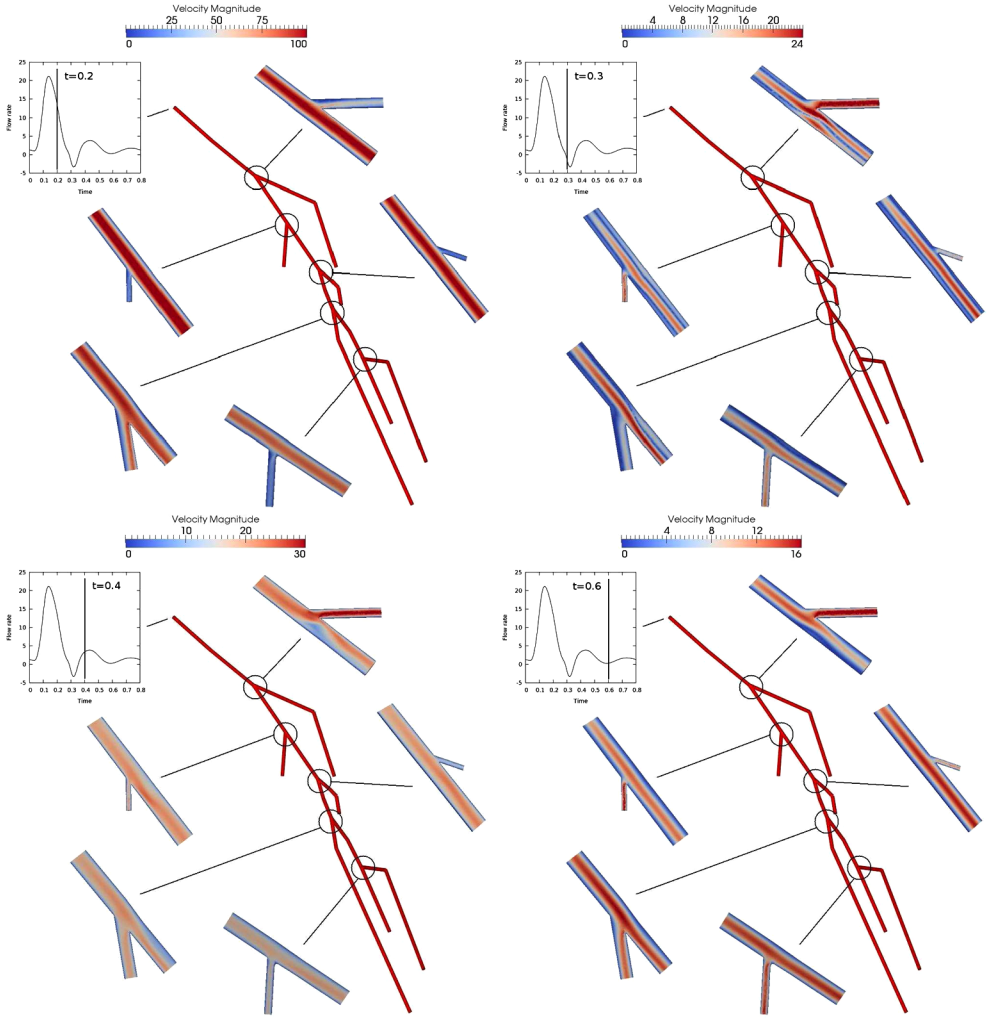

FIG. 4.18. *Velocity magnitude at different time instants through the cardiac cycle.*

Thus, the approach proposed in the present work featured high robustness as a result of employing sophisticated nonlinear solvers as well as flexibility concerning the setting of boundary conditions for the complex and simple models, something that is advantageous when compared with classical domain decomposition strategies based on Gauss–Seidel-like methods.

REFERENCES

[1] S. BERTOLUZZA, *Substructuring preconditioners for the three fields domain decomposition method*, Math. Comp., 73 (2004), pp. 659–689.

[2] P. J. BLANCO, R. A. FEIJÓO, AND S. A. URQUIZA, *A unified variational approach for coupling 3D-1D models and its blood flow applications*, Comput. Methods Appl. Mech. Engrg., 196 (2007), pp. 4391–4410.

[3] P. J. BLANCO, J. S. LEIVA, AND G. C. BUSCAGLIA, *Black-box decomposition approach for computational hemodynamics: One-dimensional models*, Comput. Methods Appl. Mech. Engrg., 200 (2011), pp. 1389–1405.

[4] P. J. Blanco, M. R. Pivello, S. A. Urquiza, and R. A. Feijóo, *On the potentialities of 3D-1D coupled models in hemodynamics simulations*, J. Biomech., 42 (2009), pp. 919–930.

[5] P. J. Blanco, S. A. Urquiza, and R. A. Feijóo, *Assessing the influence of heart rate in local hemodynamics through coupled 3D-1D-0D models*, Int. J. Num. Meth. Biomed. Engng., 26 (2010), pp. 890–903.

[6] F. Brezzi and D. Marini, *A three-field domain decomposition method*, in Domain Decomposition Methods in Science and Engineering, Contemp. Math. 157, A. Quarteroni, J. Périaux, Y. A. Kuznetsov, and O. B. Widlund, eds., American Mathematical Society, Providence, RI, 1994, pp. 27–34.

[7] R. Codina, J. Blasco, G. C. Buscaglia, and A. Huerta, *Implementation of a stabilized finite element formulation for the incompressible Navier–Stokes equation based on a pressure gradient projection*, Internat. J. Numer. Methods Fluids, 37 (2001), pp. 419–444.

[8] L. Formaggia, J. F. Gerbeau, F. Nobile, and A. Quarteroni, *On the coupling of 3D and 1D Navier–Stokes equations for flow problems in compliant vessels*, Comput. Methods Appl. Mech. Engrg., 191 (2001), pp. 561–582.

[9] L. Formaggia, J. F. Gerbeau, F. Nobile, and A. Quarteroni, *Numerical treatment of defective boundary conditions for the Navier–Stokes equations*, SIAM J. Numer. Anal., 40 (2002), pp. 376–401.

[10] L. Formaggia, F. Nobile, A. Quarteroni, and A. Veneziani, *Multiscale modelling of the circulatory system: A preliminary analysis*, Comput. Vis. Sci., 2 (1999), pp. 75–83.

[11] L. Formaggia, A. Veneziani, and C. Vergara, *Flow rate boundary problems for an incompressible fluid in deformable domains: Formulations and solution methods*, Comput. Methods Appl. Mech. Engrg., 199 (2010), pp. 677–688.

[12] J. G. Heywood, R. Rannacher, and S. Turek, *Artificial boundaries and flux and pressure conditions for the incompressible Navier–Stokes equations*, Internat. J. Numer. Methods Fluids, 22 (1996), pp. 325–352.

[13] C. T. Kelley, *Iterative Methods for Linear and Nonlinear Equations*, Frontiers Appl. Math. 16, SIAM, Philadelphia, 1995.

[14] H. J. Kim, I. E. Vignon-Clementel, C. A. Figueroa, J. F. LaDisa, K. E. Jansen, J. A. Feinstein, and C. A. Taylor, *On coupling a lumped parameter heart model and a three-dimensional finite element aorta model*, Annu. Rev. Biomed. Eng., 37 (2009), pp. 2153–2169.

[15] J. S. Leiva, P. J. Blanco, and G. C. Buscaglia, *Iterative strong coupling of dimensionally heterogeneous models*, Internat. J. Numer. Methods Engrg., 81 (2010), pp. 1558–1580.

[16] A. Quarteroni, S. Ragni, and A. Veneziani, *Coupling between lumped and distributed models for blood flow problems*, Comput. Vis. Sci., 4 (2001), pp. 111–124.

[17] A. Quarteroni and A. Veneziani, *Modeling and simulation of blood flow problems*, in Computational Science for 21st Century, Lions et al., eds., John Wiley and Sons, New York, 1997, pp. 339–350.

[18] A. Quarteroni and A. Veneziani, *Analysis of a geometrical multiscale model based on the coupling of ODEs and PDEs for blood flow simulations*, Multiscale Model. Simul., 1 (2003), pp. 173–195.

[19] S. A. Urquiza, P. J. Blanco, M. J. Vénere, and R. A. Feijóo, *Multidimensional modelling for the carotid artery blood flow*, Comput. Methods Appl. Mech. Engrg., 195 (2006), pp. 4002–4017.

[20] A. Veneziani and C. Vergara, *Flow rate defective boundary conditions in haemodynamics simulations*, Internat. J. Numer. Methods Fluids, 47 (2005), pp. 803–816.

[21] A. Veneziani and C. Vergara, *An approximate method for solving incompressible Navier–Stokes problems with flow rate conditions*, Comput. Methods Appl. Mech. Engrg., 196 (2007), pp. 1685–1700.

[22] I. E. Vignon-Clementel, C. A. Figueiroa, K. E. Jansen, and C. A. Taylor, *Outflow boundary conditions for three-dimensional finite element modeling of blood flow and pressure waves in arteries*, Comput. Methods Appl. Mech. Engrg., 195 (2006), pp. 3776–3996.